The July 2019 European heatwave in a warmer climate: Storyline scenarios with a coupled model using spectral nudging

Antonio Sánchez-Benítez,[a] Helge Goessling,[a] Felix Pithan,[a] Tido Semmler, [a] Thomas Jung,[a,b]

[a] Alfred Wegener Institute Helmholtz-Center for Polar and Marine Research, Bremerhaven, Germany.

[b] *University of Bremen, Institute of Environmental Physics, Bremen, Germany*

Corresponding author: Antonio Sánchez-Benítez, antonio.sanchez.benitez@awi.de

ABSTRACT

Extreme weather events are triggered by atmospheric circulation patterns and shaped by slower components, including soil moisture and sea-surface temperature, and by the background climate. This separation of factors is exploited by the storyline approach where an atmosphere model is nudged toward the observed dynamics using different climate boundary conditions to explore their influence. The storyline approach disregards rather uncertain climatic changes in the frequency and intensity of dynamical conditions, but focuses on the thermodynamic influence of climate on extreme events. Here we demonstrate an advanced storyline approach that employs a coupled climate model (AWI-CM-1-1-MR) where the large-scale free-troposphere dynamics are nudged toward ERA5 data. Five-member ensembles are run for present-day (2017–2019), pre-industrial, +2K, and +4K climates branching off from CMIP6 historical and scenario simulations of the same model. In contrast to previous studies, which employed atmosphere-only models, feedbacks between extreme events and the ocean and sea-ice state, and the dependence of such feedbacks on the climate, are consistently simulated. Our setup is capable of reproducing observed anomalies of relevant unconstrained parameters, including near-surface temperature, cloud cover, soil moisture, sea-surface temperature, and sea-ice concentration. Focusing on the July 2019 European heatwave, we find that the strongest warming amplification expands from southern to central Europe over the course of the 21st century. The warming reaches up to 10 K in the 4K warmer climate, suggesting that an analogous event would entail peak temperatures around 50 ºC in central Europe.

SIGNIFICANCE STATEMENT

This work explores a new storyline method to determine the impact of climate change on specific recent extreme events. The observed evolution of the large-scale atmospheric circulation is imposed in a coupled climate model. Variations in climate parameters, including ocean temperatures and sea ice, are well reproduced. By varying the background climate, including CO_2 concentrations, it is demonstrated how the July 2019 European heatwave could have evolved in pre-industrial times and in warmer climates. For example, up to 10 °C warmer peak temperatures could occur in central Europe in a 4 °C warmer climate. The method should be explored for other types of extreme events and has the potential to make climate change more tangible and to inform adaptation measures.

1. Introduction

Europe has recently experienced a number of exceptional heatwaves (e.g., Russo et al. 2015; Vautard et al. 2020). These extreme events matter for society as they are associated, among others, with extensive crop failures (Lesk et al. 2016; Beillouin et al. 2020), devastating wildfires (Sutanto et al. 2020), poor air quality (e.g., Konovalov et al. 2011; Garrido-Perez et al. 2019), and increased mortality, especially in the older people (Barriopedro et al. 2011; CRED 2020). The most extensively documented heatwaves – both in terms of studying the underlying dynamics and associated impacts – are the August 2003 heatwave over western and central Europe (e.g., Trigo et al. 2005; Russo et al. 2015; Bador et al. 2017) and the July–August 2010 event in western Russia (e.g., Barriopedro et al. 2011; Dole et al. 2011). These heatwaves redrew the temperature record map of Europe. More recently, the 2019 summer was exceptional in western and central Europe (Mitchell et al. 2019; Madruga De Brito et al. 2020; Sousa et al. 2020; Vautard et al. 2020) with two large-scale heatwaves occurring in late June and July 2019. These two extreme events were found to be the world's deadliest disaster of

2019 (CRED 2020). The former set a new record for the European-average June temperature. The most extreme daily maximum 2m air temperature (t2m) was recorded on 28 June near the city of Nimes (Verargues, 46 ºC), where a new all-time national record for France was established. The latter resulted in record-breaking temperatures in central and northern Europe. For example, the historical record of Paris was broken by more than 2 ºC (42.6 ºC); Belgium and the Netherlands for the first time surpassed the 40 ºC mark; and new national records were set in Germany, Luxembourg and the UK.

There is consensus that large-scale dynamics, characterized by subtropical ridges and blocking anticyclones associated with meandering of the jet stream, are the main driving factor for European heatwaves (e.g., Trigo et al. 2005; Jézéquel et al. 2018; Sánchez-Benítez et al. 2018; Sousa et al. 2020; Suarez-Gutierrez et al. 2020) as warm air advection from lower latitudes, solar radiative heating and subsidence are enhanced. The 2003 and 2019 heatwaves were associated with a subtropical ridge in western Europe together with a low-pressure system in the eastern Atlantic. This configuration advected hot and dry Saharian and Iberian air masses towards higher latitudes. Soil-atmosphere feedbacks impacted the strength of the heatwaves (e.g., van der Wiel et al. 2020) as they generate changes in the surface heat fluxes (Wehrli et al. 2018; Miralles et al. 2019; Sousa et al. 2020). In fact, the heatwaves in August 2003 and July 2019 were preceded by anomalously warm and dry conditions, generating a soil moisture deficit. For this type of event, other mechanisms, for example involving local SST, are believed to be of less relevance, although some controversy remains (Della-Marta et al. 2007; Duchez et al. 2016; Wehrli et al. 2019).

The Mediterranean region is often referred to as a hotspot of climate change due to a substantial amplification of global warming, especially in summer (Fischer and Schär 2010; Barcikowska et al. 2020). The amplification can partly be explained by a substantial decrease

in soil moisture availability. In future warmer climates, this lack of soil moisture – and hence the amplification – is expected to propagate northward, impacting central Europe (Vogel et al. 2017; Suarez-Gutierrez et al. 2020; Wehrli et al. 2020). Overall, it is now well established that climate change has made heatwaves more frequent, intense and prolonged (Chapman et al. 2019; Perkins-Kirkpatrick and Lewis 2020; Sánchez-Benítez et al. 2020); and this trend is expected to continue in the future (Schoetter et al. 2015; Junk et al. 2019; Suarez-Gutierrez et al. 2020).

Climate models and observations have been used to quantify how the odds of extreme temperatures that occurred during specific heatwaves have changed from the past and how much they will change in the future (e.g., Vogel et al. 2019; Zhou et al. 2019; Vautard et al. 2020). For example, an event like the July 2019 heatwave in France (Germany) is now considered to be at least ten (three) times more likely to occur than in 1900 (Vautard et al. 2020); and such an extreme event will be ~150 times more probable by the end of the century for the SSP585 scenario (i.e., 1.8 vs. 273 years return period by the end of the 21st century compared to 1950–2014; Ma et al. 2020). Despite some obvious successes of this *probabilistic approach*, as argued by Shepherd (2016), it has some limitations: Firstly, projected changes of the polar jet stream in a warmer climate are still highly uncertain (e.g., Shepherd 2014; Hoskins and Woollings 2015; Woollings et al. 2018). Hence, large ensembles are needed to provide meaningful statements. Furthermore, it is rather difficult to find good future analogues of heatwaves, not least given that in terms of impacts (e.g., on hydrology) the temporal evolution of the system prior to the heatwave is critical as well. Secondly, the probabilistic approach does not make the anticipated changes in a warming world readily accessible to the general public and some decision-makers; this is in stark contrast to so-called storyline scenarios – explored

in this study – where the impact of climate change is illustrated by considering recent extreme events that people have experienced and can connect to (Shepherd et al. 2018).

The storyline approach provides a way to disentangle dynamic from thermodynamic changes and has been explored in several recent studies (Schubert-Frisius et al. 2017; Shepherd et al. 2018; Wehrli et al. 2020; Van Garderen et al. 2021). In contrast to possible dynamic changes (e.g., meandering of the jet stream), thermodynamic changes associated with heatwaves in a warmer world are better understood and associated with relatively small uncertainty (Cattiaux et al. 2015; IPCC, 2018; Fan et al. 2020). Increasing CO2 concentrations, for example, are known to warm near-surface temperatures locally; and warmer SSTs lead to enhanced warm-air advection to downstream land regions (e.g., Dommenget 2009). In the deterministic storyline approach, heatwaves are simulated in alternative past and future climates, using an atmospheric general circulation model in which the dynamics in the free troposphere are nudged towards observations using reanalysis data. These simulations start some years before the event to appropriately capture the evolution preceding the events (e.g., spinning up soil hydrology).

So far, two different approaches were used for nudging. In Wehrli et al. (2020) the zonal and meridional winds were nudged; meanwhile, in Van Garderen et al. (2021), divergence and vorticity truncated at T20 (spectral nudging) were employed to impose the large-scale dynamical evolution. As both studies used an atmospheric circulation model, the sea-surface temperatures (SST) and sea-ice concentration (SIC) had to be prescribed. For the present-day simulations, the observed SST and SIC, including the variability possibly impacting the considered extreme events, were prescribed. For the past and future climate conditions, a climate change signal was added to the SSTs. This is a reasonable approach as it preserves the variability. However, it implies that one needs to rely on the climate change response of a

129 separate, coupled configuration of the same (or similar) atmosphere model, as in Van Garderen
130 et al. (2021), or on the response of one or more completely different climate models, as in
131 Wehrli et al. (2020). The atmosphere-only storyline approach also assumes that the impact of
132 a specific extreme event on the ocean state remains the same in different climates, neglecting
133 possible nonlinearities. Moreover, prescribing SIC poses a particular challenge because the
134 simple addition of a local climate-change signal can lead to unphysical values and, more
135 fundamentally, is not suited for the way sea ice responds to climate change by spatial migration
136 of the ice edge rather than locally continuous changes. Wehrli et al. (2020) addressed this with
137 a rather complex approach, whereas Van Garderen et al. (2021) neglected SIC changes
138 altogether. Given that their focus is on European heatwaves, however, details on how sea ice
139 is treated may not influence their conclusions.

140 The potential of the uncoupled storyline approach in capturing extreme events such as
141 the European heatwaves of 2003 and 2018 along with the Russian heatwave of 2010 has been
142 demonstrated by Wehrli et al. (2020) and Van Garderen et al. (2021). It has been shown, for
143 example, that the fraction of the AgPop region (i.e., latitudes north of 30ºN with a population
144 density above 30 km^{-2} or important for agriculture, as defined by Seneviratne et al. (2018),
145 experiencing daily maximum temperatures higher than 40 ºC in an event like the 2018
146 heatwave would quadruplicate in a future 4K warmer climate (Wehrli et al. 2020). Van
147 Garderen et al. (2021) found robust warming from preindustrial to present-day for the 2003
148 and 2010 heatwaves, with local warming of about 0–2.5 ºC (2003) and 0–4 ºC (2010). In both
149 studies, when the warming is averaged for the heatwave region, an amplified warming
150 (compared to the global-mean warming) is found, except for the 2003 heatwave.

151 The purpose of this work is to further explore and extend the storyline approach using
152 spectral nudging in a coupled model for answering three central questions: First, how would

153 the 2019 European summer and particularly the July heatwave have developed in preindustrial
154 times? Second, how might they unfold in future warmer climates (+2 and +4K)? And third, is
155 the coupled storyline approach capable of constraining the surface-ocean and sea-ice states?
156 To this end, we have run experiments with the coupled climate model AWI-CM-1.1-MR
157 (Semmler et al. 2020) with the large-scale atmospheric circulation in the free troposphere being
158 nudged to reanalysis data, while allowing thermodynamic and small-scale dynamical processes
159 to develop relatively freely. Unlike in related previous studies mentioned above, a fully coupled
160 climate model is used that contributed to the sixth phase of the Coupled Model Intercomparison
161 Project (CMIP6; Eyring et al. 2016). By branching the nudging experiments off certain states
162 from the CMIP6 trajectories (e.g., 2K warmer climate), plausible states for the sea ice-ocean
163 component of the climate system are readily available and do not need to be explicitly specified
164 like in corresponding atmosphere-only experiments. In Section 2, we define the methodology
165 used in this work, including the nudging parameters selected. In Section 3, the main results are
166 presented. In Section 4, the obtained results are briefly discussed, and the main conclusions are
167 highlighted.

168

169 **2. Methods**

170 Our simulations are based on the Alfred Wegener Institute Climate Model (AWI-CM-
171 1-1-MR, Semmler et al. 2020). This model has contributed to CMIP6 and employs the
172 atmospheric model ECHAM6.3.04p1 from MPI-M (Stevens et al. 2013) coupled to the Finite
173 Element Sea Ice-Ocean Model (FESOM) v.1.4 (Wang et al. 2014). The atmosphere model is
174 run at T127L95 spectral resolution (~100 km horizontal resolution in the tropics), with 95
175 vertical levels going up to about 0.01 hPa. The ocean mesh has a variable resolution with
176 refinement in energetically active areas such as the Gulf Stream (Sidorenko et al. 2015; Sein et

al. 2017). More specifically, ocean resolution varies from 8 to 80 km, with 8–10 km used in the North Sea, 10–12 km in the Mediterranean Sea, and 8–20 km in the Arctic (Fig. 1 in Semmler et al. 2020).

We have used spectral nudging to impose the observed large-scale circulation for certain atmospheric vertical layers. This technique forces a climate model to follow specific large-scale circulation conditions using reference data from reanalysis (Waldron et al. 1996; Von Storch et al. 2000; Zhang et al. 2014). Spectral nudging is implemented by adding an additional nudging term to the model's governing equations

$$\frac{\partial \mathrm{X}_n^m(\eta,t)}{\partial t} = \mathrm{F}_n^m(\eta,t) + \mathrm{G}_n^m(\eta)\left[\mathrm{X}_n^{m(reana)}(\eta,t) - \mathrm{X}_n^m(\eta,t)\right] \quad (1)$$

where $\mathrm{X}_n^m(\eta,t)\left(\mathrm{X}_{\mathrm{n}}^{\mathrm{m(\,reana)}}(\mathrm{\eta,t})\right)$ represents the spectral coefficient of a meteorological variable at the vertical level η and timestep t (from the reanalysis), $\mathbf{F}_n^m(\eta,t)$ the model forcing, and $\mathbf{G}_n^m(\eta)$ the nudging coefficient.

The impact of nudging depends on which meteorological variables, wavenumbers and vertical levels are constrained. In this work, only divergence and vorticity are nudged. Hence, all other variables can be freely determined by the model. For our main experiments we use a T20 triangular truncation, that is, wavenumbers for vorticity and divergence up to 20 are retained; higher-wavenumber dynamics corresponding to smaller spatial scales can be freely computed by the model. T20 was chosen since this is the lowest total wavenumber for which we found the jetstream (winds at 250 hPa) from ERA5 data (Hersbach et al. 2020) to be qualitatively and quantitatively well constrained (example shown in Fig. 1) when compared to the full field. Furthermore, we chose to only nudge model levels between 100 and 700 hPa. Sensitivity experiments with different vertical profiles of the nudging coefficient have shown that the influence of additionally constraining the stratosphere or lower troposphere is

200 negligible (Fig. 2). To avoid overfitting and allow the boundary layer to respond freely,
201 therefore, model levels above 100 hPa and below 700 hPa were not nudged in our simulations.

202 Similar to previous studies (Schubert-Frisius et al. 2017; Wehrli et al. 2018; Van
203 Garderen et al. 2021), a constant nudging strength is used for the constrained levels. To avoid
204 an abrupt transition between neighboring levels, however, the vertical nudging profile has also
205 been smoothed using a sigmoid function (Fig. S1). The nudging strength is related to an e-
206 folding time (τ), with the latter being the inverse of the former (i.e., the larger the e-folding
207 time, the weaker the nudging effect). It turns out that an e-folding time of 24 hours provides a
208 good balance between constraining the large-scale atmospheric circulation and allowing
209 differences depending on the boundary conditions to emerge. Fig. 3 shows 850 hPa winds on
210 one randomly selected day (18 July 2018) from experiments with e-folding times of 6, 24 and
211 48 hours. Results are almost indistinguishable between 6 and 24 hours, with some differences
212 emerging if an e-folding time of 48 hours is used. Hence, 24 hours appears to be a good
213 compromise between imposing the observed atmospheric flow onto the coupled climate model
214 and providing the model with a maximum of freedom to simulate relevant processes and
215 feedbacks, at least for mid-latitude heatwaves considered in this study.

216 With this configuration, we have run nudged storyline experiments using atmospheric
217 forcing fields for the period 1 January 2017 to 30 September 2019. More specifically, nudging
218 experiments with AWI-CM have been branched off the corresponding historical CMIP runs
219 (Semmler et al. 2018) on 1 January 1851 to give *pre-industrial* climate conditions; *present-day*
220 conditions were obtained by branching off the ssp370 scenario (Semmler et al. 2019) on 1
221 January 2017; and 2K and 4K warmer climates were explored by branching off the ssp370
222 scenario on 1 January 2038 and 1 January 2093, respectively (Semmler et al. 2020). For each
223 of the different time slices we have run five ensemble members.

The nudged simulations started from different ensemble members of the free-running climate model with different initial states for the atmosphere and ocean. Among others, this allows us to quantify how the different ensemble members adjust to the imposed observed forcing. Fig. 4 shows the temporal evolution of the ensemble spread of European t2m (computed as the difference between the maximum and minimum of all ensemble members for each day) for the nudging experiment under present-day conditions (similar results are obtained for other boundary conditions or variables, not shown). The ensemble spread is larger than 10 K at the beginning of the simulations; however, it reduces to about 1.5 K within the first few months, suggesting that the first few months should be discarded from the analysis for atmospheric fields. Nevertheless, we allow for one year of spin-up time to reach a stabilization for more slowly responding parameters such as soil moisture, sea-ice concentration and SST. Accordingly, where not stated otherwise, simulations with the large-scale dynamical conditions for the period 1 January 2018 to 30 September 2019 prescribed for pre-industrial, present-day, and 2K as well as 4K warmer climates are analyzed.

Similar to previous studies (e.g., Takhsha et al. 2018; Wehrli et al. 2019), we have found that the global model climatology is not strongly affected by the nudging, with differences within the ensemble spread (not shown). Furthermore, the AWI-CM-1-1-MR free-runs from the CMIP6 archive have been used to compute climatologies (e.g., to determine anomalies and explore weather-dependent amplification of climate change).

3. Results

3.1 Assessment of the nudged simulations for Europe under present-day conditions

Before discussing the storyline scenarios, we compare the present-day nudged simulations with ERA5. Here we focus on Europe; section 3.3 provides an assessment for Arctic sea ice.

An example for nudged simulations compared to ERA5 data is given for the 25 July 2019 (peak of the heatwave; Fig. 5) before we turn to a quantitative analysis. The anomalous circulation in the coupled climate model on that day, expressed in terms of 500 hPa geopotential height (Z500), is an excellent analogue of the observed blocking conditions. The same is true for parameters such as temperature at 850 hPa (T850) and maximum t2m, which are not directly constrained by the spectral nudging. Overall, the observed characteristics of the heatwave over northwestern Europe are thus well captured. As discussed in more detail below, there is evidence that maximum t2m are slightly underestimated in some regions impacted by the heatwave (Fig. 5e,f). Anomalies of SST and soil moisture at level 1 (SML1) associated with this extreme event are also well captured, confirming that climate anomalies associated with central European heatwaves are strongly driven by atmospheric circulation anomalies. Even fields like total cloud cover (TCC) are reasonably well captured in the Euro-Atlantic region by the nudged simulations for present-day conditions (Fig. 5k,l), suggesting the cloud physical processes are not negatively influenced by the nudging of vorticity and divergence.

There are some mismatches between the storyline simulations and ERA5 for this particular day (e.g., in the Balkans, central Iberia and some Arctic regions), noting, however, that for parameters like TCC or SML1 the reanalysis itself is not necessarily well constrained by direct observations. Overall, our results give confidence that the storyline setup with the coupled model captures key processes related to European heatwaves – including atmospheric blocking, warm air advection, clear skies and soil moisture deficits – if driven by large-scale wind fields from ERA5 in the free troposphere.

So far, our assessment has focused on one particular day at the peak of the July 2019 heatwave. For a more comprehensive assessment, correlations between our storyline simulations for present-day conditions and ERA5 as a proxy for observations for the summers of 2018 and 2019 are shown in Fig. 6. Sizeable correlations are obtained for critical variables that are not nudged in our simulations. We have repeated the correlation analysis after having removed low-frequency variability, including the seasonal cycle (i.e., removing a 15-day running mean prior to the analysis). Even for highpass-filtered data, correlations remain high with values exceeding 0.6 for all parameters except soil moisture which is probably more influenced by local convective processes (Fig. S2). In summary, therefore, our methodology does not only work well for single extreme cases; more generally, it also captures daily to seasonal variability in Europe during summertime.

This point is further illustrated by Fig. 7, which shows the simulated and reanalyzed maximum, minimum and mean t2m time series for Europe and Germany for the period 1 June to 31 August 2019 (see the definition of these areas in Fig. S3). For both regions, the nudged simulations capture the variability very well. In fact, correlations between simulated and reanalyzed time series mostly exceed r=0.9. For Europe, however, some differences emerge on longer seasonal time scales: While the climate model tends to slightly underestimate t2m in early June, during the course of the summer positive t2m biases emerge. Further analysis suggests that there are small pan-European cold biases in early summer, turning into larger warm biases in southeastern Europe from late June (Fig. S4). The time series for Germany (Fig. 7) generally indicates smaller maximum t2m biases for the coupled model. However, there is some evidence for the exceptionally warm periods in June and July 2019 to be underestimated – especially for maximum t2m during daytime. On the other hand, the coupled model simulates realistic t2m for the third heatwave in late August 2019. Our analysis suggests

that the biases are flow-dependent and that there may be even differences between individual extreme events. In this context, it can be argued that the spectral nudging approach – like more sophisticated data assimilation methods such as 4D-Var (e.g., Rodwell and Palmer 2007) – has strong diagnostic potential to help unravel the causes of biases in coupled climate models at the process level, thus guiding model development.

To further explore the flow-dependence of the t2m biases for Germany, we have selected the ten days with the strongest positive and strongest negative max t2m differences for Germany between our nudged simulations and ERA5 (Fig. 8), using summer data from 2018 and 2019. The most striking finding from this analysis is that the climate model tends to underestimate the maximum t2m during heatwaves in Germany, which are governed by the presence of a pronounced anomalous anticyclonic circulation anomaly, and thus strong European blocking events. No such coherent atmospheric circulation anomaly is found for periods when the simulated t2m in Germany are warmer than in the reanalysis (Fig. 8a,c,e). The finding that the nudged model underestimates extreme t2m during heatwaves in Germany is important, especially when it comes to making quantitative statements on the impact of heatwaves and their future changes.

3.2 Storyline scenarios for the European summer of 2019

Having demonstrated that the spectral nudging approach with the coupled climate model works well, we now analyze how the summer of 2019, including the July heatwave, might have evolved in pre-industrial times and how it might unfold in future 2K and 4K warmer climates. For Germany, there is very robust warming for maximum and minimum t2m (i.e., the ensembles for different climates do not overlap) that tends to grow throughout the summer season – from pre-industrial times to the present and from present-day to 4K warmer climates

(Fig. 9). Changes in maximum and minimum t2m from present-day conditions (approximately +1.2K in the storyline experiments) to a 2K warmer climate are smaller, even though they are still quite robust in terms of the separation of the two ensembles. In general, these findings are consistent with the free-running CMIP6 simulations (dashed lines in Fig. 9), suggesting that they are not a particular feature of this specific summer.

Another point illustrated by Fig. 9 is that in nighttime t2m (minimum t2m) in Germany in a 4K warmer world are projected to become comparable to typical daytime maxima (maximum t2m) in pre-industrial times – at least for the heatwaves that occurred in late July and August 2019.

Remarkably, this anthropogenic warming in Germany has an intraseasonal cycle (Fig. S5 for maximum t2m with similar results for minimum t2m, not shown), with values close to the global average in early summer, and increasing relative to global value in mid and late summer. In fact, values around +5.5 K (+4K minus present-day), +0.8 K (+2K minus present-day) and +2.0 K (present-day minus pre-industrial) are obtained for the July heatwave peak. Hence, there is evidence for global warming amplification in phase with the July event, particularly in the 4K warmer climate (2-fold increase). Similar results can be found in the free run, so this amplification is not specific to the events in July 2019. When the differences are computed for +2K minus pre-industrial and +4K minus +2K, then non-significantly higher warming is obtained for the latter (Fig. S5, bottom). This suggests that there might be some feedback mechanisms generating a slightly higher than expected warming in the future.

The European heatwaves during the summer of 2019 did not only impact land areas; they were also accompanied by ocean heatwaves in the North Sea, as demonstrated in Fig. 10, which shows the evolution of SST in the North Sea and the German Bight (see their definition in Fig. S3). Generally, the ocean heatwaves are more pronounced for the latter region. This is

not too surprising given that it represents a smaller and shallow area that lies closer to the area most impacted by the heatwaves. Around mid-July, SST in the German Bight is about 1 K cooler in the nudged runs compared to the climatological signal derived from the free runs; shortly before the 25 July, anomalies turn positive, reaching about +2 K in late July and early August. Thus, the impact of heatwaves on SST in both areas suggests that using coupled climate models for storyline scenarios may be an advantage when it comes to capturing events that are impacted by coupled processes.

From a climatological point of view, the warming of SST in the German Bight from pre-industrial times to the 4K warmer world amounts to about 4 K. This is quite a substantial change compared to SST changes in the open ocean (~3 K). The ocean heatwave in early August, for example, would have been accompanied by SSTs of about 20 ºC in pre-industrial times; in a 4K warmer world SSTs could reach up to 24 ºC. The change is probably even larger in the shallow waters closer to the coast not resolved by the climate model (~8 km is used in the North Sea). Furthermore, it is worth pointing out that, compared to t2m, for SST changes there is even less evidence for a warming acceleration when comparing the warming from +2K to +4K against the warming from pre-industrial times to +2K (Fig. A6). This is consistent with an earlier finding that the observed warming in the North Sea during the last few decades was quite strong (Wiltshire et al. 2010).

The evolution of SST warming in the nudged 2019 storyline simulations exhibits some interesting differences compared to the corresponding climatological warming. For example, considering the change from present-day to the 4K warmer climate, SSTs in the German Bight increase by about 0.5 K more in the storyline runs in June 2019 compared to the climatological warming, whereas the opposite holds for August 2019 (Fig. S6), resulting in a dampened strength of the late-summer heatwaves (Fig. 10). This provides evidence for a dependence of

366 the SST climate-change signal on weather patterns which could not be captured by storyline
367 scenarios using atmospheric models with prescribed SSTs.

368 Spatial maps of the t2m differences on 25 July 2019 between the different climates for
369 the wider European region are shown in Fig. 11. These maps describe the "warming signal of
370 the day", given the large-scale circulation and its evolution during the preceding days, weeks
371 and months. Some well-known climate change features (e.g., Fischer and Schär 2010;
372 Barcikowska et al. 2020; Suarez-Gutierrez et al. 2020) emerge for this particular day: For
373 example, extreme temperatures over land areas tend to increase more strongly than those over
374 the ocean; the warming is more pronounced in southern Europe compared to more northern
375 regions of continental Europe; and the warming signal tends to move northward during the 21st
376 century. Furthermore, anomalously strong warming signals can be found locally in some of the
377 regions (e.g., northeastern Spain and southwestern France), which supports the notion that there
378 may be some "weather-dependent amplification" of climate change. However, not all of the
379 small-scale structures may be due to this weather dependence. Some of the differences may
380 simply be "random", for example depending on the presence of clouds (less well constrained
381 and thus more uncertain) and hence the strength of the incoming solar radiation.

382 From Fig. 11 it can also be inferred that for some regions in Germany, the additional
383 warming from present-day conditions to the end of the 21st century (4K warmer world) would
384 amount to as much as 7 K. By adding the 3.6 K experienced today compared to pre-industrial
385 times, locally maximum t2m by the end of the century could exceed 47 ºC; in contrast,
386 maximum t2m would have stayed below 37 ºC in pre-industrial times – certainly extreme, but
387 not necessarily dangerously high (see Fig. 18 in the Discussion and conclusions section).

388 We have also explored the connection between changes in t2m, soil wetness and Bowen
389 ratio, which is defined as the ratio of sensible to latent heat fluxes. The seasonal evolution of

soil wetness and the Bowen ratio in the different climates is shown in Fig. 12. The summer of 2019 starts with anomalously dry soils that were comparable for the different climates (i.e., the ensembles show some overlap). Furthermore, latent heat flux dominates over sensible heat flux in June, as indicated by the Bowen ratios remaining below 0.5 for all climates. Driven by the first heatwave in late June 2019 (Fig. 9), a dramatic decrease in soil wetness is witnessed in all simulations, with values reaching the 5th quantile obtained from the CMIP6 (dotted lines in Fig. 12). The more moderate conditions in early and mid-July led to a minor increase in soil wetness. As a consequence, the July heatwave occurred with anomalously, but not exceptionally dry soils (below the 4K warmer climate climatology). In early July, the reduced soil moisture availability triggered an increase in Bowen ratio to values around 1. Nevertheless, after a small decrease in mid-July, the values on the heatwave peak are only slightly higher than the climatology. This suggests that dry soils exacerbated the July heatwave but were not a key factor.

Remarkably, the consequences of the June event in both variables are even greater in the 4K warmer climate, with robustly drier conditions and a higher Bowen ratio from early July to the end of the season. Thus, these higher changes in the radiative fluxes (due to a lack of soil moisture) can partly explain the larger warming amplification observed in this area in the future 4K warmer climate. Therefore, a heatwave in early summer (as in 2003 or 2019) could exacerbate a heatwave occurring later (high summer) as it creates dry soil conditions that intensify the second event by changes in the surface heat fluxes. Furthermore, at least for the 2019 summer, this effect would be stronger in the 4K warmer climate than in the preindustrial to 2K warmer climates.

Maps of soil wetness and Bowen ratio for 25 July 2019 are shown in Fig. 13. They help to explain the global warming amplification and non-linear changes found for t2m. From the

pre-industrial to present-day climates, there is a strong and robust drying in the Mediterranean region which is accompanied by a dramatic increase in Bowen Ratio. Meanwhile, in central and northern Europe differences are relatively small due to the availability of sufficient soil moisture. When considering future changes (i.e., +4K minus present-day) the drying of the soil and the increase in Bowen ratio peak in mid-latitude regions, including central Europe

.

3.3 Storyline scenarios for Arctic sea ice

The use of a coupled model allows studying coupled environmental extreme events, as mentioned in Section 3.2 for SST in the North Sea. Here we provide some initial insight into the value of the coupled storyline scenario approach for Arctic sea ice. In general, studying sea-ice anomalies in a coupled storyline approach might be useful not only to explore more directly sea-ice related extremes, such as the opening of polynyas north of Greenland (Moore et al. 2018; Ludwig et al. 2019); sea-ice anomalies have also been shown to influence mid-latitude events, such as extreme snowfall in northern Europe, through modification of air masses (Bailey et al. 2021). Here we therefore briefly discuss how Arctic sea-ice anomalies and changes are represented in our coupled storyline simulations, acknowledging that sea ice probably had a minor role to play when it comes to thermodynamic processes driving European heatwaves.

Daily anomalies of the pan-Arctic sea-ice extent (area with SIC > 15%) are relatively coherent between the nudged simulation and ERA5 (Fig. 14). Omitting the first year, where the model state might still be affected by the spin-up, the Pearson correlation for the ensemble mean is ~0.65 (~0.53 if the first year is included). While some of the strong anomalies are clearly captured, in particular during the second half of 2018, some anomalies are not well captured by the nudged simulation. In particular, observed negative anomalies around April

both in 2018 and 2019 are in contrast to positive anomalies in the storyline simulations. However, it is worth noting that the ensemble spread during these inconsistent periods is much larger than during the second half of 2018, suggesting that the sea-ice state may be less strongly constrained by the large-scale circulation in the early melt season compared to other times of the year.

Another factor that can lead to inconsistent anomalies is model bias. While this probably holds for any quantity, it may be particularly influential for the sea-ice state. Moderate temperature biases, for example, can lead to significant errors in the ice-edge location. As a consequence, the ice-edge location in a biased model will respond differently to the same large-scale circulation anomaly pattern, simply because the ice edge resides in a different place. Indeed, AWI-CM free runs exhibit non-negligible biases in the ice-edge location (Semmler et al. 2020), and nudging only the large-scale dynamics does not – and is not meant to – rectify thermodynamically-induced model biases. In July, for example, the climatological ice edge extends much further into the Barents and Kara Seas in AWI-CM compared to ERA5 (black contours in Fig. 15). However, despite these limitations, the regional patterns of sea-ice concentration anomalies tend to be captured rather well. For example, during the Arctic melt season 2019 on 25 July (the peak of the central European heatwave), negative SIC anomalies prevailed in the Chukchi, East Siberian, and Laptev Seas, whereas positive anomalies prevailed in (or north of) the Barents and Beaufort Seas (Fig. 15, bottom). While the moderately negative pan-Arctic sea-ice extent anomaly at that time is not reproduced (the simulated anomalies are near-neutral; Fig. 14), the spatial patterns are reasonably well captured (Fig. 15, top).

The fact that the ice edge responds differently to large-scale circulation anomalies depending on where it resides on average is even more important when it comes to sea-ice anomalies in significantly different climates: The climatological sea-ice distributions in the

462 pre-industrial, present, +2K, and +4K climates are vastly different (Fig. 16). For example, one
463 cannot expect that a large-scale circulation pattern that causes, or at least contributes to, a
464 record-low pan-Arctic sea-ice extent in pre-industrial or present climate would have a similar
465 effect in a 4K warmer climate, where scarcely any Arctic sea ice remains even in July (Fig.
466 16), two months before the end of the classical melt season. This may complicate the
467 assessment to what extent sea-ice anomalies associated with a specific extreme event may
468 amplify or dampen some aspects of the event when transferred to a different climate. However,
469 as it is the case for SSTs, it is arguably more physically consistent regarding the two-way
470 interaction of sea ice with an extreme event to simulate the sea-ice response in a coupled model
471 rather than to prescribe the sea-ice state and its response in some non-trivial way.

472

473 **4. Discussion and Conclusions**

474 In this study we present a method for computing storyline scenarios using spectral
475 nudging in a coupled climate model. The strength of this approach lies in the use of a coupled
476 climate model that has contributed to CMIP6 (i.e., AWI-CM-1-1-MR, Semmler et al. 2020).
477 By using a coupled approach one can study climate and environmental extremes in a coupled
478 framework, thereby avoiding possible shortcomings that arise from having to specify SST and
479 sea-ice conditions for past and future climates. In this context, the availability of CMIP6
480 simulations, from which the nudging experiments can be branched off, is a distinct advantage.
481 By applying a scale-dependent, spectral nudging approach in the free troposphere only, as in
482 Van Garderen et al. (2021), it is possible to constrain only the large-scale circulation associated
483 with the jet stream, which is known to be one of the key drivers of extreme and high-impact
484 environmental events in mid-latitudes.

485 The full potential of this approach can further be inferred from Fig. 17, illustrating
486 coupled storyline scenarios for 1600 UTC 20 September 2019 – another event in late
487 summer/early autumn 2019. This confirms that (i) the jet stream, i.e., the dynamically driver,
488 is realistically represented; (ii) anthropogenic warming is strongest over land, especially when
489 considering changes from present-day condition to a 4K warmer world; (iii) locally extreme
490 SSTs anomalies (i.e., ocean heatwaves) emerge in the Mediterranean Sea, with SSTs
491 exceeding +30 ºC in the central Mediterranean Sea; and (iv) there are vastly different sea-ice
492 conditions in the Arctic that are consistent with the atmospheric state and its previous evolution.
493 We should note that the last two points are treated in a physically more consistent way in
494 coupled storyline scenarios than it could by prescribing SST and SIC fields in atmosphere-only
495 storyline scenarios.

496 The storyline approach, employing nudging, is computationally quite efficient, at least
497 once CMIP-type simulations are available from which nudged simulations can be branched off.
498 This is due to the fact that the main source of uncertainty in future projections of European
499 extreme events – that is strong internal atmospheric variability compared to relatively weak
500 climate change signals – has been effectively "removed" by prescribing the temporal evolution
501 of the large-scale mid-troposphere dynamics. In fact, in agreement with Wehrli et al. (2020)
502 and Van Garderen et al. (2021), for European heatwaves just a few ensemble members are
503 sufficient to separate signal from noise, once the evolution of the large-scale atmospheric
504 circulation is prescribed.

505 As pointed out by Shepherd et al. (2018), storyline scenarios provide a very effective
506 way of making the impacts of climate change more tangible to experts and non-experts alike
507 – thus facilitating decision-making in adaptation and mitigation. This point is further illustrated
508 in Fig. 18, showing "weather maps" of t2m during the peak of this record-breaking heatwave

in Germany in July 2019 for present-day, pre-industrial and future conditions: While this weather event was clearly extreme by nature, with maximum t2m of about 37 ºC even without anthropogenic warming, the warming since pre-industrial times made it record-breaking (42 ºC in places) with substantial impacts on society, businesses and infrastructure, including a "meltdown" of the German railway system. In a 4K warmer world (i.e., 3 K warmer than today) daytime t2m would be reaching dangerously high values, nearing 50 ºC. The value of this approach for understanding and communicating the impact of climate change could be further enhanced by using these storyline scenarios to drive impact models. In this way, it would become possible to draw more complete "pictures", for example by also making statements about surface hydrology, river levels and the state of the vegetation.

It seems likely that finding analogs of similar quality from observations, CMIP data and large ensembles will be difficult, if possible at all. This is especially true if the temporal dimension is taken into account, which is critical when it comes to parameters such as soil moisture and SST that memorize past weather and are not only of interest in their own right but also feedback on temperatures during the evolution of heatwaves.

The coupled storyline approach, presented in this study, also provides a very powerful way of diagnosing the origin of model error at the process level, thus guiding future model development. Usually, one of the main challenges in diagnosing coupled models arises from the fact that a direct comparison with observations from field campaigns, which are usually comprehensive and of high quality but limited in time, is difficult to carry out. Therefore, disentangling differences due to different weather from those due to model deficiencies becomes difficult. Recognizing this, activities such as Transpose-CMIP – that is, running short-term predictions with initialized coupled climate models – have been proposed and applied (e.g., Voldoire et al. 2019). Here we argue that the storyline simulations, using spectral nudging

in climate models, provide another promising way of analyzing model shortcomings, including those that occur only sporadically during certain weather types (i.e., flow-dependent biases). To explore this idea further, we are planning to extend the experiments until the end of 2020 and provide a thorough comparison with observational data from the MOSAiC expedition – the year-round drift through the Arctic which lasted from October 2019 to October 2020. Related to this, the approach proposed in this study provides a powerful technique to understand and quantify how coupled processes associated with certain phenomena (e.g., heatwaves, sea-ice polynyas and cold-air outbreaks) change in different climates. The fact that dry soils in southern Europe at the end of the 21st century in a 4K warmer world are projected to change the role of how the atmosphere interacts with the soil is a promising example.

Storyline scenarios are in principle not limited to specific types of events. However, it is likely not a coincidence that studies demonstrating the approach so far have been focussing on heatwaves; these have a rather large-scale footprint and can thus be reproduced relatively easily by constraining the large-scale dynamics. While the same may hold for cold-extremes in winter, events that occur on smaller scales and involve small-scale dynamics and fronts, including extreme rainfall events like the devastating flash floods in western Germany in July 2021, are more challenging. In our setup, where the nudging is relatively weak and leaves wavenumbers above 20 free, extreme rains are clearly underestimated (not shown). Dedicated efforts are needed to extend the storyline approach to different types of events. It is possible that different event types will require different optimal settings, and that events with a strong small-scale random component may necessitate a large-ensemble storyline approach.

To summarize, this work presents the first storyline of the European July 2019 heatwave augmenting previous probabilistic attribution studies (Ma et al. 2020; Vautard et al. 2020) in which changes of the frequency of occurrence of certain events in different climates

are quantified. The most outstanding finding of this study is the global warming amplification found associated with the July 2019 heatwave (locally up to 4-fold increase). This amplification is enhanced and northward displaced in the future 4K warmer climate, with more than a 2-fold increase in Germany (both for maximum and minimum t2m). In contrast with the result obtained by Van Garderen et al. (2021) for the European 2003 heatwave, an amplification is also found from preindustrial to present climate (an ~1.5-fold increase in Germany), with the highest warming found in the Mediterranean region. The warming obtained for the 2019 summer is similar to the climatological mean warming, as may be due to a climatological drying of soils comparable to the drying that occurred during the 2019 summer. In addition, we have not found significant flow-dependent stronger or weaker changes in our simulations (not shown). However, this last result should be assessed using simulations that span longer periods, e.g., starting in 1979. Meanwhile, neither a future global warming amplification nor a summer intraseasonal cycle of warming is found for SST in our study areas, more specifically, the North Sea. However, the observed SST warming there is close to the global warming and thus stronger than the mean ocean-surface warming.

Overall, our study adds further support to the notion that storyline scenarios provide a promising approach that augments traditional probabilistic approaches to the attribution of extreme events and that help to make climate change and its impact more tangible to scientists, decision-makers and the general public.

Acknowledgments.

This work was supported by the Helmholtz-Klima-Initiative through the HI-CAM project (Drivers cluster). HFG acknowledges the financial support by the Federal Ministry of Education and Research of Germany in the framework of SSIP (grant 01LN1701A). The

simulations were performed at the German Climate Computing Center (DKRZ) using the esm-tools (Barbi et al. 2021). We thank Sebastian Rast (MPI-M) for support with the spectral nudging in ECHAM, Michael Böttinger (DKRZ) for the Fig 17 and 18 visualizations, and the ESM-Tools staff for their assistance during the simulation.

Data Availability Statement.

Data from the AWI-CM-1-1-MR free runs are available in the Earth System Grid Federation (ESGF) data nodes (e.g. https://esgf-data.dkrz.de/search/cmip6-dkrz/). The nudging experiments are stored in the supercomputer Mistral from DKRZ and will be shared soon in a public repository. ERA5 reanalysis data used in this study can be accessed from the European Center for Medium-Range Weather Forecasts (ECMWF; https://www.ecmwf.int/en/forecasts/datasets/reanalysis-datasets/era5).

603 REFERENCES

604 Bador, M., L. Terray, J. Boé, S. Somot, A. Alias, A. L. Gibelin, and B. Dubuisson, 2017: Future
605 summer mega-heatwave and record-breaking temperatures in a warmer France climate.
606 *Environ. Res. Lett.*, **12**, 074025, https://doi.org/10.1088/1748-9326/aa751c.

607 Bailey, H., A. Hubbard, E. S. Klein, K.-R. Mustonen, P. D. Akers, H. Marttila, and J. M.
608 Welker, 2021: Arctic sea-ice loss fuels extreme European snowfall. *Nat. Geosci.*, **14**, 283–
609 288, https://doi.org/10.1038/s41561-021-00719-y.

610 Barbi, D., N. Wieters, P. Gierz, M. Andrés-Martínez, D. Ural, F. Chegini, S. Khosravi, and L.
611 Cristini, 2021: ESM-Tools version 5.0: a modular infrastructure for stand-alone and
612 coupled Earth system modelling (ESM). *Geosci. Model Dev.*, **14**, 4051–4067,
613 https://doi.org/10.5194/gmd-14-4051-2021.

614 Barcikowska, M. J., S. B. Kapnick, L. Krishnamurty, S. Russo, A. Cherchi, and C. K. Folland,
615 2020: Changes in the future summer Mediterranean climate: contribution of
616 teleconnections and local factors. *Earth Syst. Dyn.*, **11**, 161–181,
617 https://doi.org/10.5194/esd-11-161-2020.

618 Barriopedro, D., E. M. Fischer, J. Luterbacher, R. M. Trigo, and R. García-Herrera, 2011: The
619 Hot Summer of 2010: Redrawing the Temperature Record Map of Europe. *Science*, **332**,
620 220–224, https://doi.org/10.1126/science.1201224.

621 Beillouin, D., B. Schauberger, A. Bastos, P. Ciais, and D. Makowski, 2020: Impact of extreme
622 weather conditions on European crop production in 2018. *Philos. Trans. Roy. Soc. B Biol.*
623 *Sci.*, **375**, 20190510, https://doi.org/10.1098/rstb.2019.0510.

624 Cattiaux, J., H. Douville, R. Schoetter, S. Parey, and P. Yiou, 2015: Projected increase in
625 diurnal and interdiurnal variations of European summer temperatures. *Geophys. Res. Lett.*,
626 **42**, 899–907, https://doi.org/10.1002/2014GL062531.

627 Centre for research on the epidemiology of disasters (CRED), 2020: Natural disasters 2019:
628 Now is the time to not give up, 8pp, https://cred.be/sites/default/files/adsr_2019.pdf.

629 Chapman, S. C., N. W. Watkins, and D. A. Stainforth, 2019: Warming Trends in Summer
630 Heatwaves. *Geophys. Res. Lett.*, **46**, 1634–1640, https://doi.org/10.1029/2018GL081004.

631 Della-Marta, P. M., M. R. Haylock, J. Luterbacher, and H. Wanner, 2007: Doubled length of
632 western European summer heat waves since 1880. *J. Geophys. Res: Atmospheres*, **112**,
633 D15103, https://doi.org/10.1029/2007JD008510.

634 Dole, R., and Coauthors, 2011: Was there a basis for anticipating the 2010 Russian heat wave?
635 *Geophys. Res. Lett.*, **38**, L06702, https://doi.org/10.1029/2010GL046582.

636 Dommenget, D., 2009: The Ocean's Role in Continental Climate Variability and Change. *J.*
637 *Climate*, **22**, 4939–4952, https://doi.org/10.1175/2009JCLI2778.1.

638 Duchez, A., and Coauthors, 2016: Drivers of exceptionally cold North Atlantic Ocean
639 temperatures and their link to the 2015 European heat wave. *Environ. Res. Lett.*, **11**,
640 074004, https://doi.org/10.1088/1748-9326/11/7/074004.

641 Eyring, V., S. Bony, G. A. Meehl, C. A. Senior, B. Stevens, R. J. Stouffer, and K. E. Taylor,
642 2016: Overview of the Coupled Model Intercomparison Project Phase 6 (CMIP6)
643 experimental design and organization. *Geosci. Model Dev.*, **9**, 1937–1958,
644 https://doi.org/10.5194/gmd-9-1937-2016.

Fan, X., Q. Duan, C. Shen, Y. Wu, and C. Xing, 2020: Global surface air temperatures in CMIP6: historical performance and future changes. *Environ. Res. Lett.*, **15**, 104056, https://doi.org/10.1088/1748-9326/abb051.

Fischer, E. M., and C. Schär, 2010: Consistent geographical patterns of changes in high-impact European heatwaves. *Nat. Geosci.*, **3**, 398–403, https://doi.org/10.1038/ngeo866.

Garrido-Perez, J. M., C. Ordóñez, R. García-Herrera, and J. L. Schnell, 2019: The differing impact of air stagnation on summer ozone across Europe. *Atmos. Environ.*, **219**, 117062, https://doi.org/10.1016/j.atmosenv.2019.117062.

Hersbach, H., and Coauthors, 2020: The ERA5 global reanalysis. *Quart. J. Roy. Meteor. Soc.*, **146**, 1999–2049, https://doi.org/10.1002/qj.3803.

Hoskins, B., and T. Woollings, 2015: Persistent Extratropical Regimes and Climate Extremes. *Curr. Climate Change Rep.*, **1**, 115–124, https://doi.org/10.1007/s40641-015-0020-8.

IPCC, 2018: Global Warming of 1.5°C. An IPCC Special Report on the impacts of global warming of 1.5°C above pre-industrial levels and related global greenhouse gas emission pathways, in the context of strengthening the global response to the threat of climate change, sustainable development, and efforts to eradicate poverty, V.Masson-Delmotte et al., Eds.. 630 pp, https://www.ipcc.ch/site/assets/uploads/sites/2/2019/06/SR15_Full_Report_High_Res.pdf

Jézéquel, A., P. Yiou, and S. Radanovics, 2018: Role of circulation in European heatwaves using flow analogues. *Climate Dyn.*, **50**, 1145–1159, https://doi.org/10.1007/s00382-017-3667-0.

666 Junk, J., K. Goergen, and A. Krein, 2019: Future Heat Waves in Different European Capitals
667 Based on Climate Change Indicators. *Int. J. Environ. Res. Public. Health*, **16**, 3959,
668 https://doi.org/10.3390/ijerph16203959.

669 Konovalov, I. B., M. Beekmann, I. N. Kuznetsova, A. Yurova, and A. M. Zvyagintsev, 2011:
670 Atmospheric impacts of the 2010 Russian wildfires: integrating modelling and
671 measurements of an extreme air pollution episode in the Moscow region. *Atmos. Chem.*
672 *Phys.*, **11**, 10031–10056, https://doi.org/10.5194/acp-11-10031-2011.

673 Lesk, C., P. Rowhani, and N. Ramankutty, 2016: Influence of extreme weather disasters on
674 global crop production. *Nature*, **529**, 84–87, https://doi.org/10.1038/nature16467.

675 Ludwig, V., G. Spreen, C. Haas, L. Istomina, F. Kauker, and D. Murashkin, 2019: The 2018
676 North Greenland polynya observed by a newly introduced merged optical and passive
677 microwave sea-ice concentration dataset. *Cryosphere*, **13**, 2051–2073,
678 https://doi.org/10.5194/tc-13-2051-2019.

679 Ma, F., X. Yuan, Y. Jiao, and P. Ji, 2020: Unprecedented Europe Heat in June–July 2019: Risk
680 in the Historical and Future Context. *Geophys. Res. Lett.*, **47**, e2020GL087809,
681 https://doi.org/10.1029/2020GL087809.

682 Madruga De Brito, M., C. Kuhlicke, and A. Marx, 2020: Near-real-time drought impact
683 assessment: a text mining approach on the 2018/19 drought in Germany. *Environ. Res.*
684 *Lett.*, **15**, 1040a9, https://doi.org/10.1088/1748-9326/aba4ca.

685 Miralles, D. G., P. Gentine, S. I. Seneviratne, and A. J. Teuling, 2019: Land–atmospheric
686 feedbacks during droughts and heatwaves: state of the science and current challenges. *Ann.*
687 *N. Y. Acad. Sci.*, **1436**, 19–35, https://doi.org/10.1111/nyas.13912.

688 Mitchell, D., K. Kornhuber, C. Huntingford, and P. Uhe, 2019: The day the 2003 European
689 heatwave record was broken. *Lancet Planet. Health*, **3**, e290–e292,
690 https://doi.org/10.1016/S2542-5196(19)30106-8.

691 Moore, G. W. K., A. Schweiger, J. Zhang, and M. Steele, 2018: What Caused the Remarkable
692 February 2018 North Greenland Polynya? *Geophys. Res. Lett.*, **45**, 13,342-13,350,
693 https://doi.org/10.1029/2018GL080902.

694 Perkins-Kirkpatrick, S. E., and S. C. Lewis, 2020: Increasing trends in regional heatwaves. *Nat.*
695 *Commun.*, **11**, 1–8, https://doi.org/10.1038/s41467-020-16970-7.

696 Rodwell, M. J., and T. N. Palmer, 2007: Using numerical weather prediction to assess climate
697 models. *Quart. J. Roy. Meteor. Soc.*, **133**, 129–146, https://doi.org/10.1002/qj.23.

698 Russo, S., J. Sillmann, and E. M. Fischer, 2015: Top ten European heatwaves since 1950 and
699 their occurrence in the coming decades. *Environ. Res. Lett.*, **10**, 124003,
700 https://doi.org/10.1088/1748-9326/10/12/124003.

701 Sánchez-Benítez, A., R. García-Herrera, D. Barriopedro, P. M. Sousa, and R. M. Trigo, 2018:
702 June 2017: The Earliest European Summer Mega-heatwave of Reanalysis Period. *Geophys.*
703 *Res. Lett.*, **45**, 1955–1962, https://doi.org/10.1002/2018GL077253.

704 ——, D. Barriopedro, and R. García-Herrera, 2020: Tracking Iberian heatwaves from a new
705 perspective. *Wea. Climate Extrem.*, **28**, 100238,
706 https://doi.org/10.1016/j.wace.2019.100238.

707 Schoetter, R., J. Cattiaux, and H. Douville, 2015: Changes of western European heat wave
708 characteristics projected by the CMIP5 ensemble. *Climate Dyn.*, **45**, 1601–1616,
709 https://doi.org/10.1007/s00382-014-2434-8.

Schubert-Frisius, M., F. Feser, H. von Storch, and S. Rast, 2017: Optimal spectral nudging for global dynamic downscaling. *Mon. Wea. Rev.*, **145**, 909–927, https://doi.org/10.1175/MWR-D-16-0036.1.

Sein, D. V., and Coauthors, 2017: Ocean Modeling on a Mesh With Resolution Following the Local Rossby Radius. *J. Adv. Model. Earth Syst.*, **9**, 2601–2614, https://doi.org/10.1002/2017MS001099.

Semmler, T., and Coauthors, 2018: AWI AWI-CM1.1MR model output prepared for CMIP6 CMIP historical. https://doi.org/10.22033/ESGF/CMIP6.2686.

——, and Coauthors, 2019: AWI AWI-CM1.1MR model output prepared for CMIP6 ScenarioMIP ssp370. https://doi.org/10.22033/ESGF/CMIP6.2803.

——, and Coauthors, 2020: Simulations for CMIP6 With the AWI Climate Model AWI-CM-1-1. *J. Adv. Model. Earth Syst.*, **12**, 1–34, https://doi.org/10.1029/2019MS002009.

Seneviratne, S. I., and Coauthors, 2018: Land radiative management as contributor to regional-scale climate adaptation and mitigation. *Nat. Geosci.*, **11**, 88–96, https://doi.org/10.1038/s41561-017-0057-5.

Shepherd, T. G., 2014: Atmospheric circulation as a source of uncertainty in climate change projections. *Nat. Geosci.*, **7**, 703–708, https://doi.org/10.1038/NGEO2253.

——, 2016: A Common Framework for Approaches to Extreme Event Attribution. *Curr. Climate Change Rep.*, **2**, 28–38, https://doi.org/10.1007/s40641-016-0033-y.

729 ——, and Coauthors, 2018: Storylines: an alternative approach to representing uncertainty in
730 physical aspects of climate change. *Climate Change*, **151**, 555–571,
731 https://doi.org/10.1007/s10584-018-2317-9.

732 Sidorenko, D., and Coauthors, 2015: Towards multi-resolution global climate modeling with
733 ECHAM6–FESOM. Part I: model formulation and mean climate. *Climate Dyn.*, **44**, 757–
734 780, https://doi.org/10.1007/s00382-014-2290-6.

735 Sousa, P. M., D. Barriopedro, R. García-Herrera, C. Ordóñez, P. M. M. Soares, and R. M.
736 Trigo, 2020: Distinct influences of large-scale circulation and regional feedbacks in two
737 exceptional 2019 European heatwaves. *Commun. Earth Environ.*, **1**, 48,
738 https://doi.org/10.1038/s43247-020-00048-9.

739 Stevens, B., and Coauthors, 2013: Atmospheric component of the MPI-M earth system model:
740 ECHAM6. *J. Adv. Model. Earth Syst.*, **5**, 146–172, https://doi.org/10.1002/jame.20015.

741 Suarez-Gutierrez, L., W. A. Müller, C. Li, and J. Marotzke, 2020: Dynamical and
742 thermodynamical drivers of variability in European summer heat extremes. *Climate Dyn.*,
743 **54**, 4351–4366, https://doi.org/10.1007/s00382-020-05233-2.

744 Sutanto, S. J., C. Vitolo, C. Di Napoli, M. D'Andrea, and H. A. J. Van Lanen, 2020: Heatwaves,
745 droughts, and fires: Exploring compound and cascading dry hazards at the pan-European
746 scale. *Environ. Int.*, **134**, 105276, https://doi.org/10.1016/j.envint.2019.105276.

747 Takhsha, M., O. Nikiéma, P. Lucas-Picher, R. Laprise, L. Hernández-Díaz, and K. Winger,
748 2018: Dynamical downscaling with the fifth-generation Canadian regional climate model
749 (CRCM5) over the CORDEX Arctic domain: effect of large-scale spectral nudging and of

empirical correction of sea-surface temperature. *Climate. Dyn.*, **51**, 161–186, https://doi.org/10.1007/s00382-017-3912-6.

Trigo, R. M., R. García-Herrera, J. Díaz, I. F. Trigo, and M. A. Valente, 2005: How exceptional was the early August 2003 heatwave in France? *Geophys. Res. Lett.*, **32**, L10701, https://doi.org/10.1029/2005GL022410.

van der Wiel, K., F. M. Selten, R. Bintanja, R. Blackport, and J. A. Screen, 2020: Ensemble climate-impact modelling: extreme impacts from moderate meteorological conditions. *Environ. Res. Lett.*, **15**, 034050, https://doi.org/10.1088/1748-9326/ab7668.

Van Garderen, L., F. Feser, and T. G. Shepherd, 2021: A methodology for attributing the role of climate change in extreme events: A global spectrally nudged storyline. *Nat. Hazards Earth Syst. Sci.*, **21**, 171–186, https://doi.org/10.5194/nhess-21-171-2021.

Vautard, R., and Coauthors, 2020: Human contribution to the record-breaking June and July 2019 heatwaves in Western Europe. *Environ. Res. Lett.*, **15**, https://doi.org/10.1088/1748-9326/aba3d4.

Vogel, M. M., R. Orth, F. Cheruy, S. Hagemann, R. Lorenz, B. J. J. M. van den Hurk, and S. I. Seneviratne, 2017: Regional amplification of projected changes in extreme temperatures strongly controlled by soil moisture-temperature feedbacks. *Geophys. Res. Lett.*, **44**, 1511–1519, https://doi.org/10.1002/2016GL071235.

——, J. Zscheischler, R. Wartenburger, D. Dee, and S. I. Seneviratne, 2019: Concurrent 2018 Hot Extremes Across Northern Hemisphere Due to Human-Induced Climate Change. *Earths Future*, **7**, 692–703, https://doi.org/10.1029/2019EF001189.

771 Voldoire, A., and Coauthors, 2019: Evaluation of CMIP6 DECK Experiments With CNRM-
772 CM6-1. *J. Adv. Model. Earth Syst.*, **11**, 2177–2213,
773 https://doi.org/10.1029/2019MS001683.

774 Von Storch, H., H. Langenberg, and F. Feser, 2000: A spectral nudging technique for
775 dynamical downscaling purposes. *Mon. Wea. Rev.*, **128**, 3664–3673,
776 https://doi.org/10.1175/1520-0493(2000)128<3664:ASNTFD>2.0.CO;2.

777 Waldron, Kim. M., J. Paegle, and J. D. Horel, 1996: Sensitivity of a Spectrally Filtered and
778 Nudged Limited-Area Model to Outer Model Options. *Mon. Wea. Rev.*, **124**, 529–547,
779 https://doi.org/10.1175/1520-0493(1996)124<0529:SOASFA>2.0.CO;2.

780 Wang, Q., S. Danilov, D. Sidorenko, R. Timmermann, C. Wekerle, X. Wang, T. Jung, and J.
781 Schröter, 2014: The Finite Element Sea Ice-Ocean Model (FESOM) v.1.4: Formulation of
782 an ocean general circulation model. *Geosci. Model Dev.*, **7**, 663–693,
783 https://doi.org/10.5194/gmd-7-663-2014.

784 Wehrli, K., B. P. Guillod, M. Hauser, M. Leclair, and S. I. Seneviratne, 2018: Assessing the
785 Dynamic Versus Thermodynamic Origin of Climate Model Biases. *Geophys. Res. Lett.*, **45**,
786 8471–8479, https://doi.org/10.1029/2018GL079220.

787 ——, ——, ——, ——, and S. I. Seneviratne, 2019: Identifying Key Driving Processes of
788 Major Recent Heat Waves. *J. Geophys. Res. Atmospheres*, **124**, 11746–11765,
789 https://doi.org/10.1029/2019JD030635.

790 ——, M. Hauser, and S. I. Seneviratne, 2020: Storylines of the 2018 Northern Hemisphere
791 heatwave at pre-industrial and higher global warming levels. *Earth Syst. Dyn.*, **11**, 855–
792 873, https://doi.org/10.5194/esd-11-855-2020.

Wiltshire, K. H., and Coauthors, 2010: Helgoland Roads, North Sea: 45 Years of Change. *Estuaries Coasts*, **33**, 295–310, https://doi.org/10.1007/s12237-009-9228-y.

Woollings, T., and Coauthors, 2018: Blocking and its Response to Climate Change. *Curr. Clim. Change Rep.*, **4**, 287–300, https://doi.org/10.1007/s40641-018-0108-z.

Zhang, K., and Coauthors, 2014: Technical note: On the use of nudging for aerosol-climate model intercomparison studies. *Atmos. Chem. Phys.*, **14**, 8631–8645, https://doi.org/10.5194/acp-14-8631-2014.

Zhou, C., K. Wang, D. Qi, and J. Tan, 2019: Attribution of a record-breaking heatwave event in summer 2017 over the yangtze river delta. *Bull. Amer. Meteor. Soc.*, **100**, S97–S103, https://doi.org/10.1175/BAMS-D-18-0134.1.

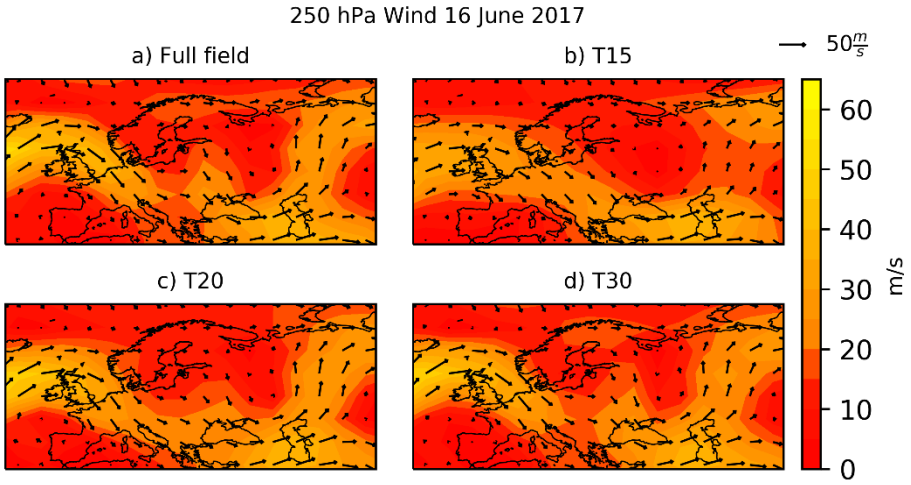

815
816
817 Figure 1. Daily mean winds at 250 hPa on 16 June 2017 from ERA5 for (a) the original field
818 and for truncated fields retaining only total wavenumbers up to (b) 15, (c) 20 and (d) 30.

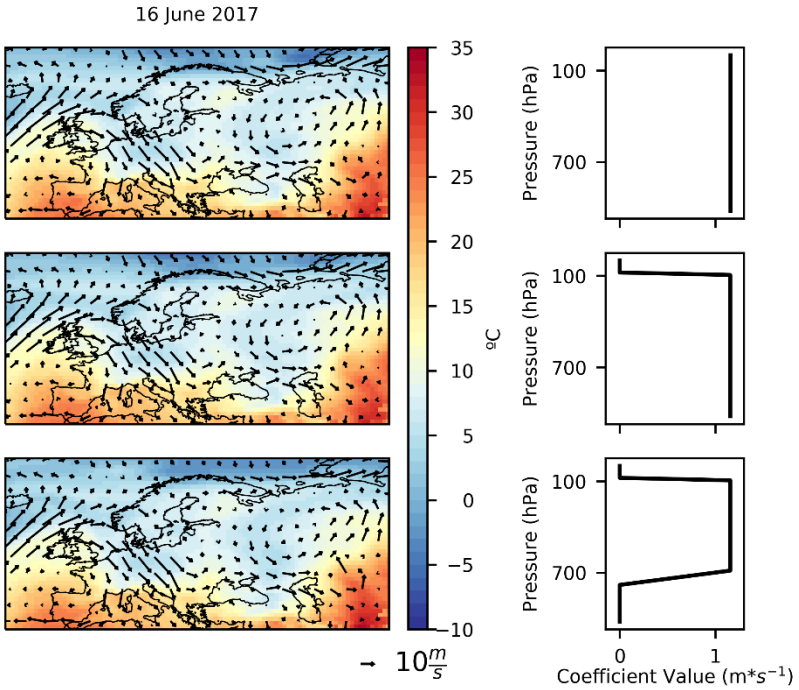

819

820 Figure 2. Daily mean temperature (shading) and winds (arrows) at 850 hPa on 16 June 2017
821 (left) for different vertical profiles indicated in the right panels. For all simulations vorticity
822 and divergence were nudged up to total wavenumber 20 with a nudging time scale of $\boldsymbol{\tau}$=24h.

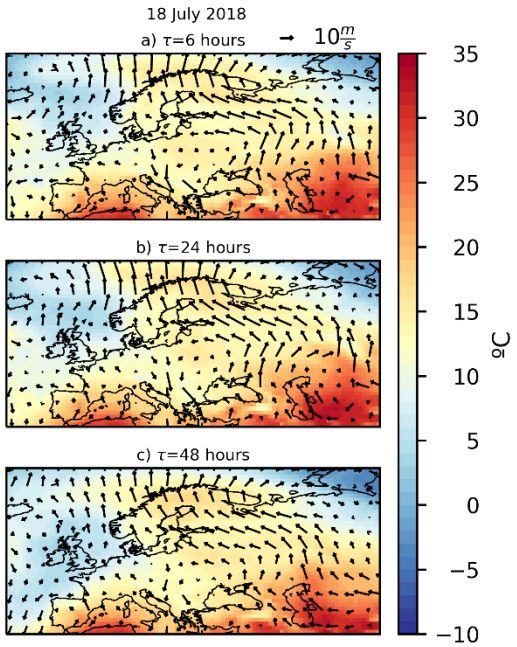

823

824 Figure 3. Temperature (shading) and winds (arrows) at 850 hPa on 18 July 2018 using different
825 e-folding times: (a) 6 hours, (b) 24 hours, and (c) 48 hours. For all simulations vorticity and
826 divergence were nudged up to total wavenumber 20 using the vertical profile shown in the
827 lower right panel of Fig. 2.

828

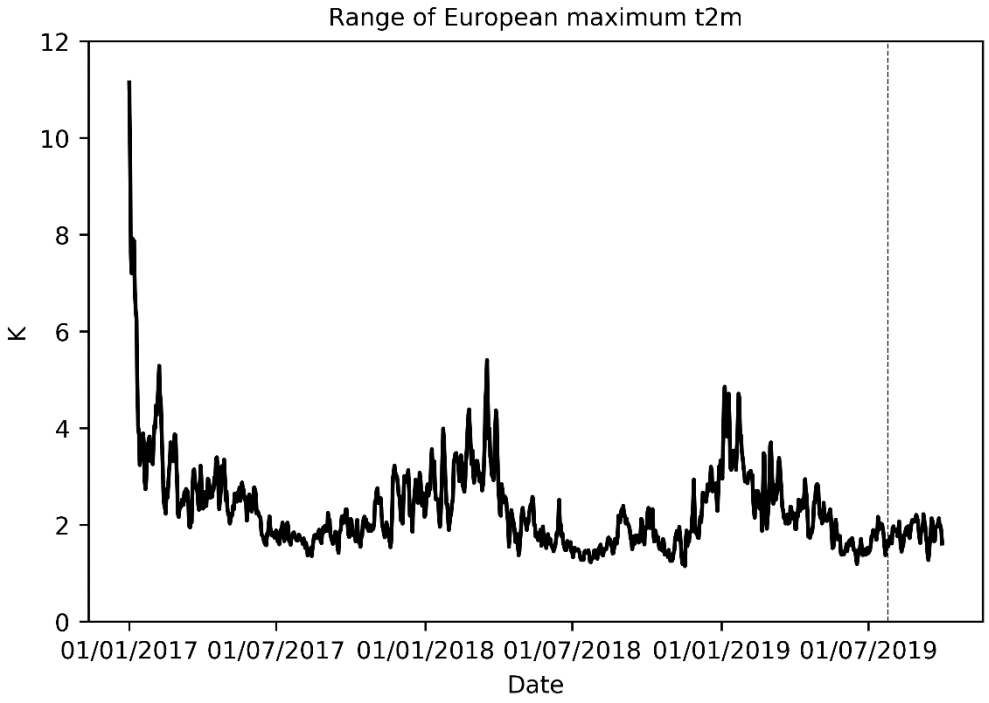

829

830 Figure 4. Temporal evolution of the range of daily maximum t2m for Europe (See Fig. A3d
831 for more details on the region). The range is computed as the difference between the daily
832 maximum and minimum values of the five ensemble members for each day. Larger values
833 indicate that maximum t2m is less well constrained by the nudging. The peak of the
834 European heatwave on 25 July 2019 is marked by the vertical dashed line.

835

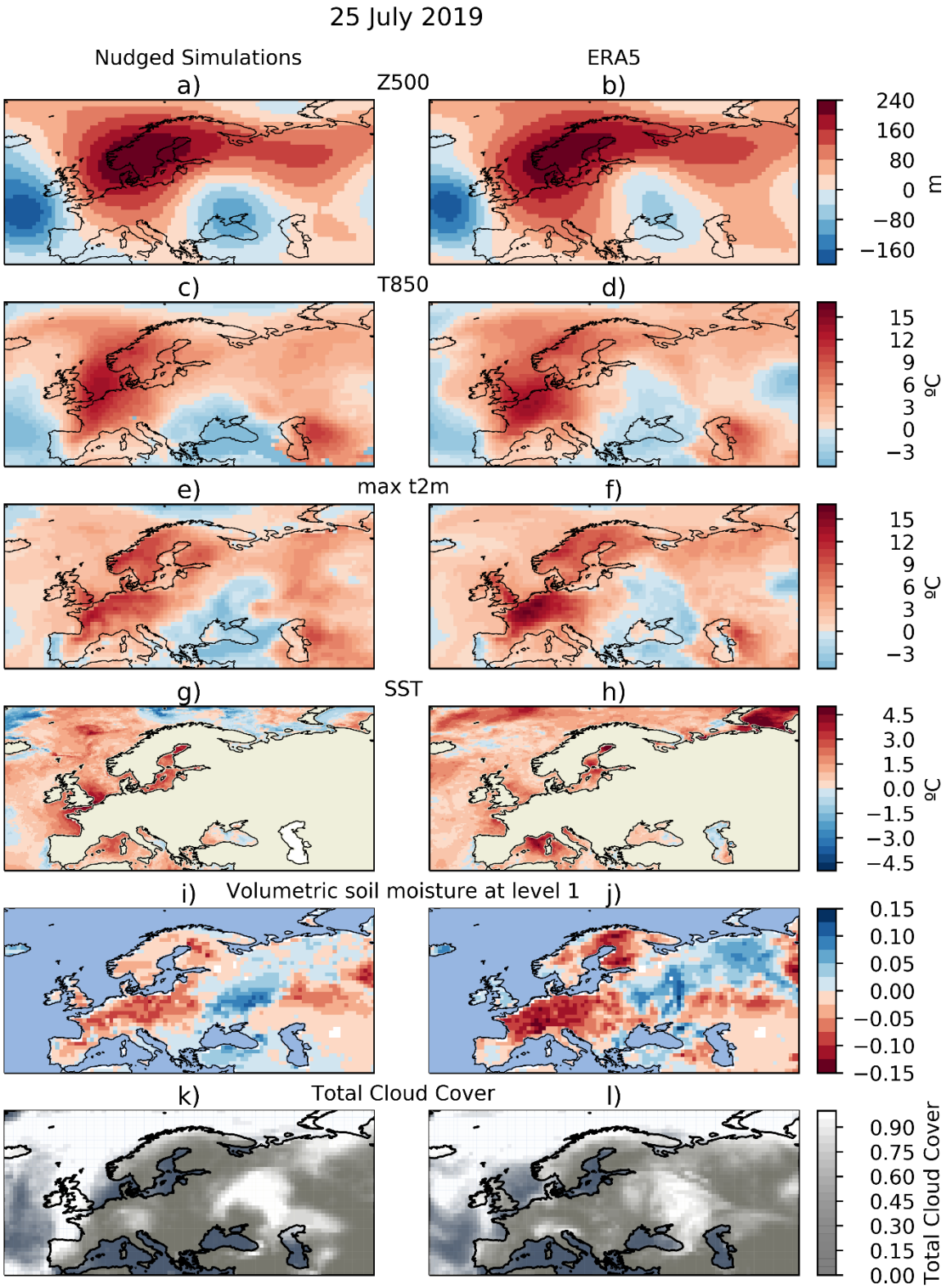

836

837 Figure 5. Anomalies from (a,c,e,g,i) the nudged present-day simulations and (b,d,f,h,j,l) ERA5

838 for 25 July 2019 and different variables: (a,b) 500 hPa geopotential height, (c,d) 850 hPa

temperature (e,f) maximum 2m temperature, (g,h) sea surface temperature, and (i,j) volumetric soil moisture in the 1st layer. Anomalies were computed as the differences of daily value from the 15-days moving average in the 1981–2010 period. Total cloud cover on 25 July 2019 for (k) the nudged present-day simulations and (l) ERA5.

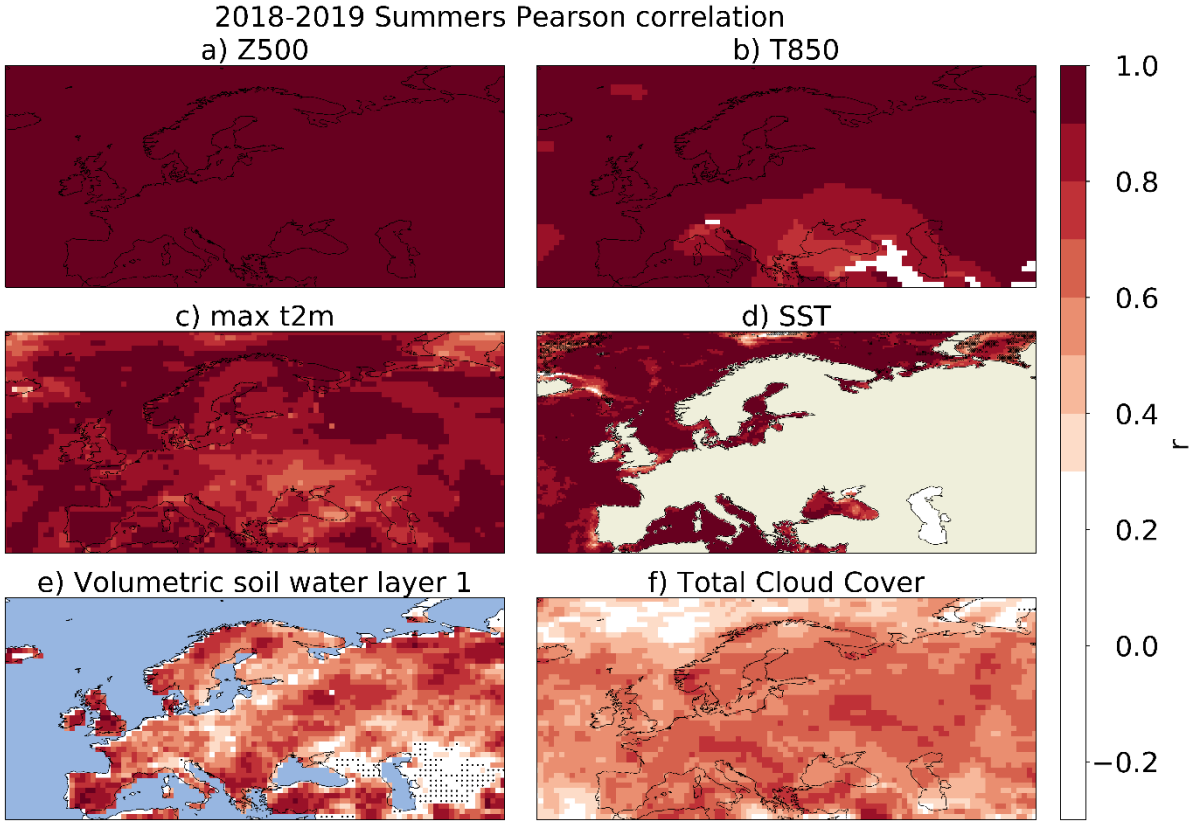

Figure 6. Pearson correlation between present-day simulations and ERA5 for the summers of 2018 and 2019 using daily fields: (a) 500 hPa geopotential height, (b) 850 hPa temperature, (c) maximum 2m temperature, (d) sea surface temperature, (e) volumetric soil moisture in the 1st layer, (f) total cloud cover. Grid points with non-significant correlation are shown with dots.

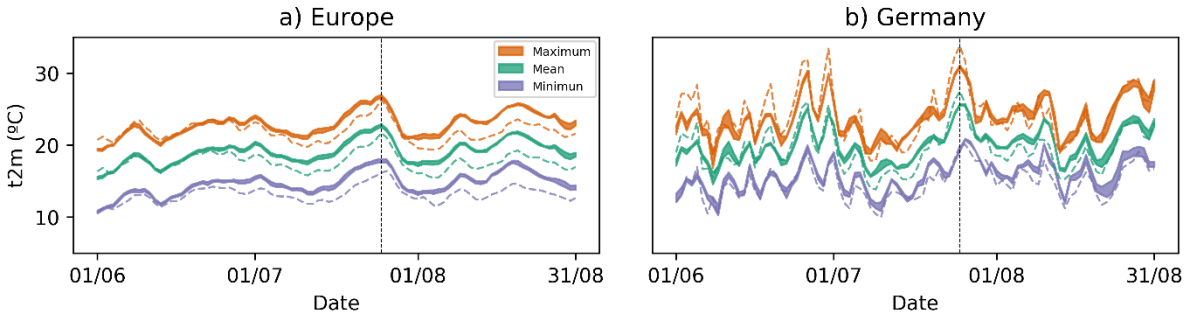

852

853 Figure 7. Seasonal evolution of daily minimum (purple), daily mean (green) and daily
854 maximum (orange) 2m temperature for (a) Europe and (b) Germany and the period 1 June to
855 31 August 2019. Results are shown for the nudged simulations under present-day conditions
856 (shading) as well as for ERA5 reanalysis data (dashed lines). Shading denotes the min/max
857 range of values obtained from the respective 5-member ensembles. The peak of the European
858 heatwave on 25 July 2019 is marked by the vertical dashed line.

859

860

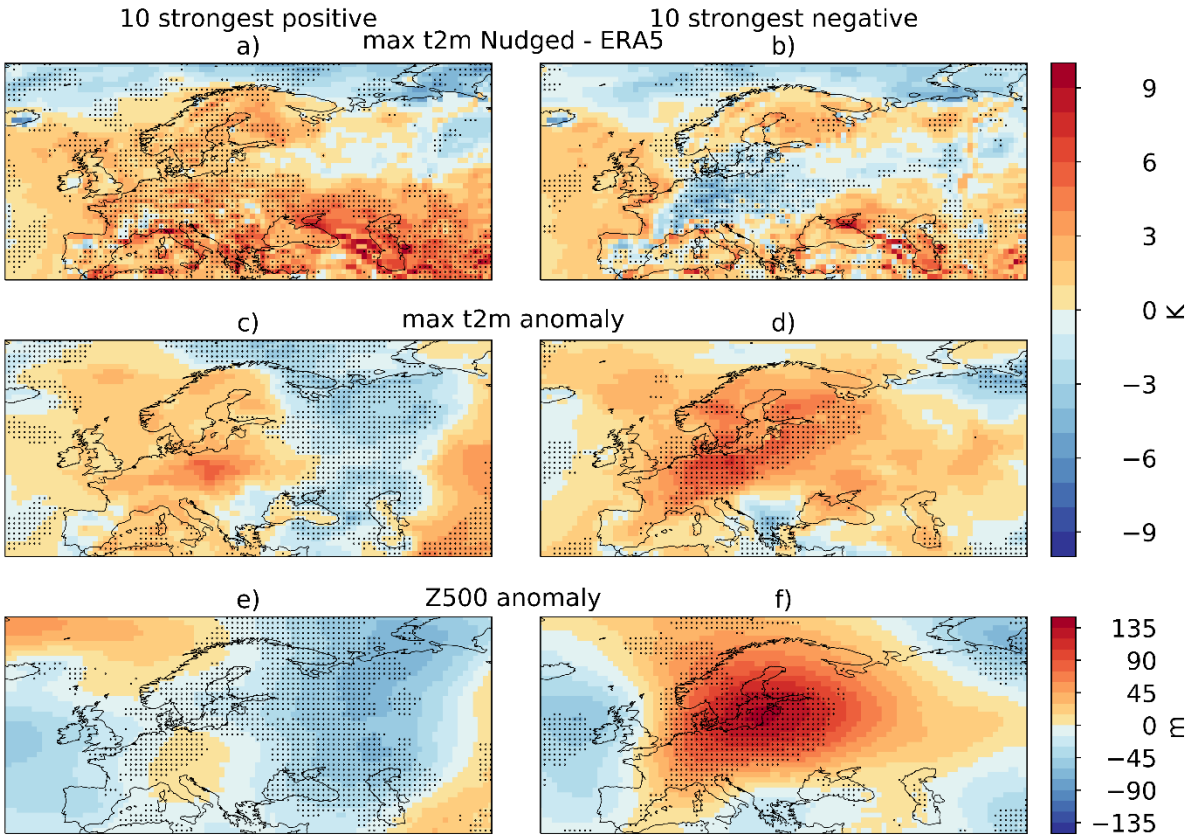

Figure 8. (a,b) max t2m differences between the nudged present-day simulations and ERA5, (c,d) max t2m anomaly and (e,f) Z500 anomaly for the ten days with (a,c,e) strongest positive and (b,d,f) negative Germany maximum t2m differences between the simulations and ERA5. The summers of 2018 and 2019 were included. Grid points where the differences are significant are shown with points.

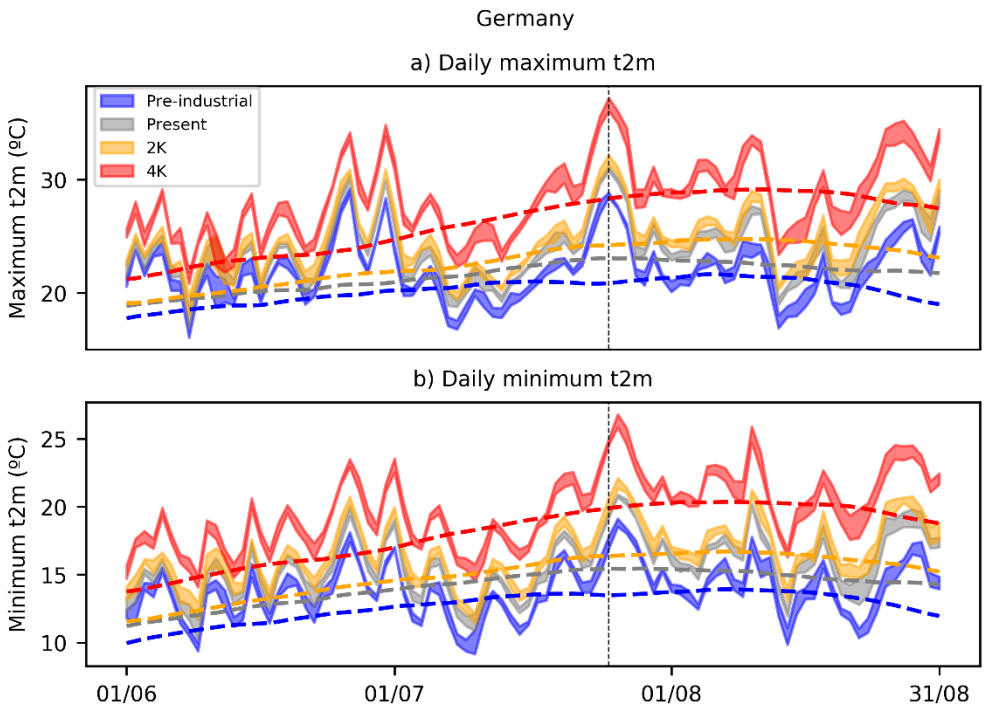

872

873 Figure 9. Seasonal evolution of (a) daily maximum and (b) minimum t2m averaged for
874 Germany and different climates (pre-industrial in blue, present-day in grey, +2K in orange and
875 +4K in red). Shading spans the min/max range of values obtained from the 5-member
876 ensembles and dashed lines show the mean from the free-run. Differences are shown in Fig.
877 A5. The peak of the European heatwave on 25 July 2019 is marked by the vertical dashed line.

878

879

880

881

882

883

884

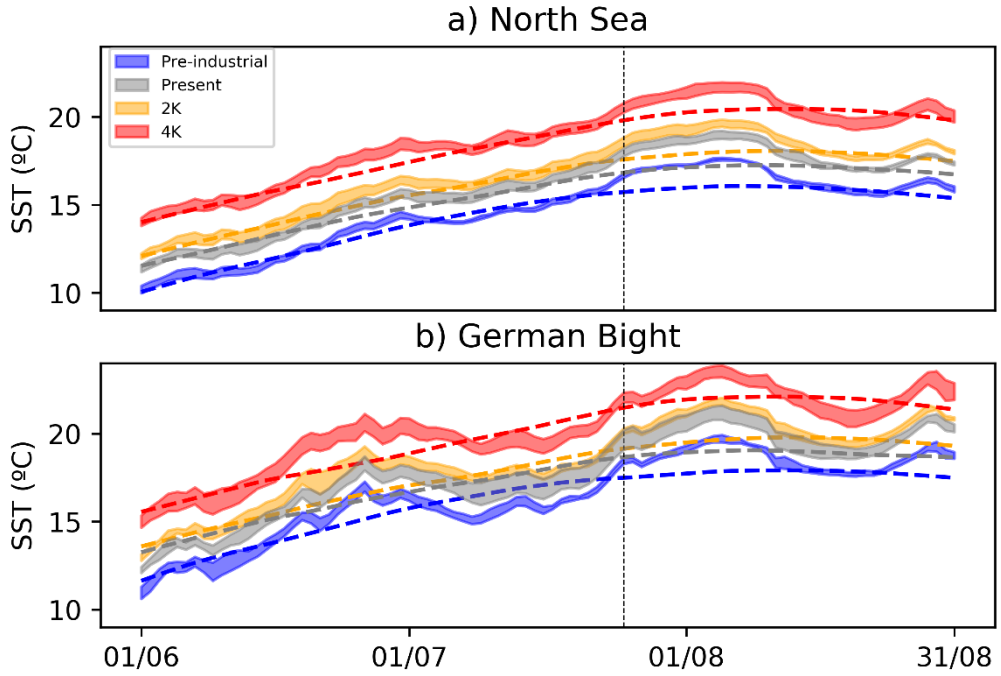

Figure 10. Same as Fig. 9, except for sea surface temperature in (a) the North Sea and (b) the German Bight. The peak of the European heatwave on 25 July 2019 is marked by the vertical dashed line.

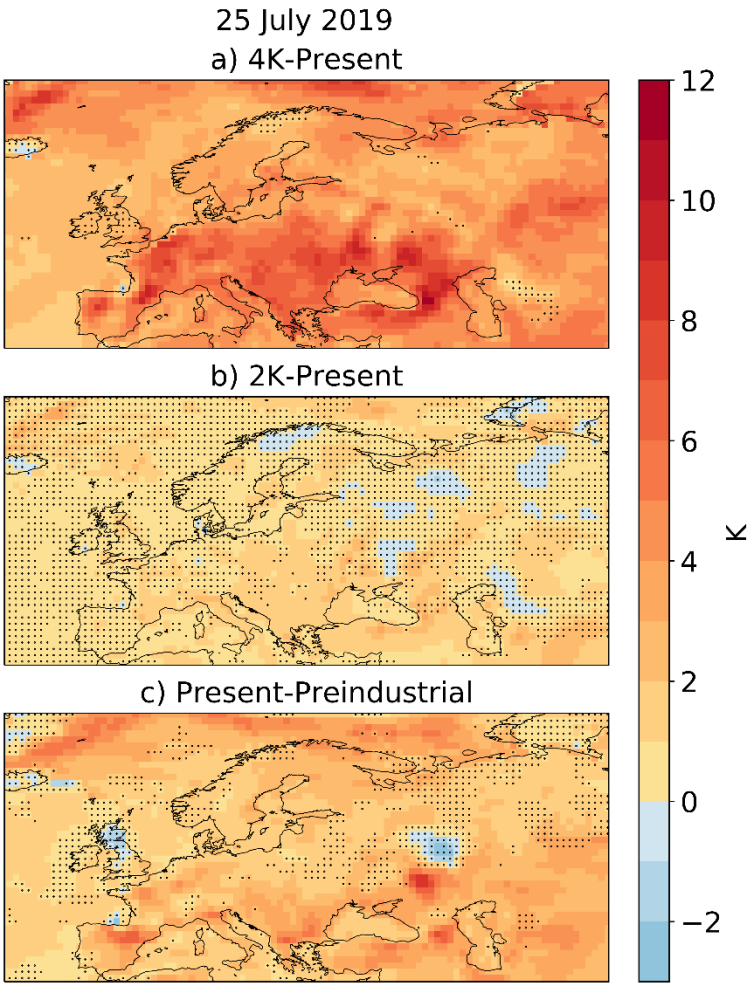

Figure 11. Daily maximum t2m differences on 25 July 2019: (a) +4K minus present-day, (b) +2K minus present-day, and (c) present-day minus pre-industrial. Locations where the ensembles overlap between different climates are indicated with points.

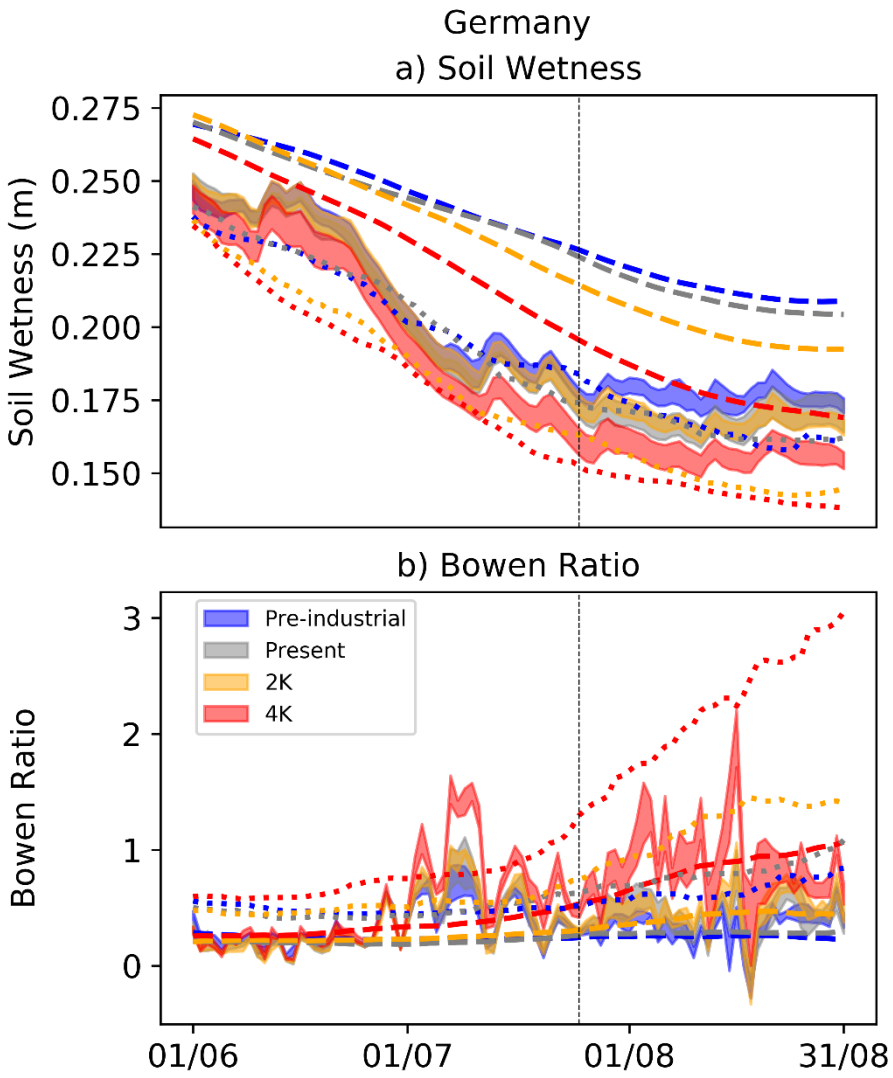

906

907 Figure 12. Seasonal evolution of (a) soil wetness and (b) Bowen ratio in Germany between 1
908 June to 31 August 2019 in different climates (pre-industrial in blue, present-day in yellow and
909 2K and 4K warmer worlds in orange and red, respectively). Shading spans the min/max range
910 of values obtained by the respective 5-member ensembles. Dashed lines show the mean and
911 dotted lines the 5th and 95th quantile for Soil Wetness and Bowen Ratio respectively. The
912 peak of the European heatwave on 25 July 2019 is marked by the vertical dashed line.

913

914

915

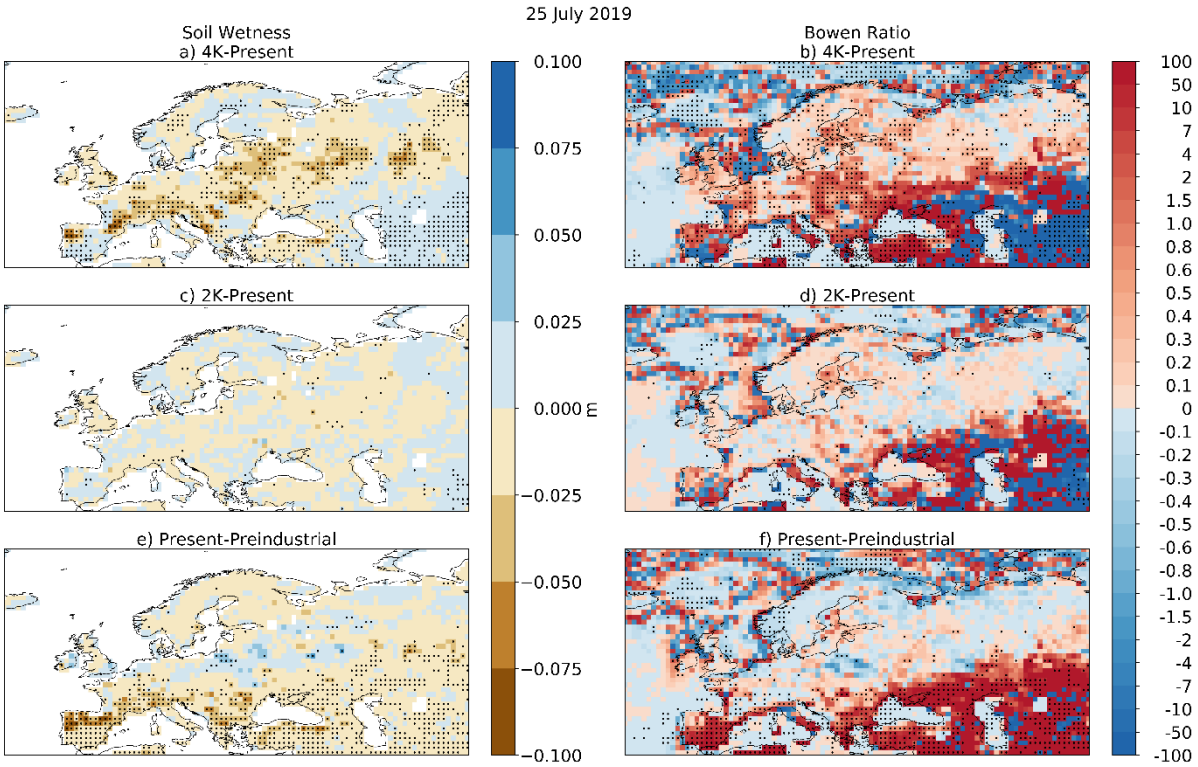

916

917 Figure 13. (a,c,e) Soil wetness and (b,d,f) Bowen ratio differences between (a,b) 4K warmer
918 and present, (c,d) 2K warmer and present and (e,f) present and preindustrial climates on 25
919 July 2019. Locations where the two ensembles do not overlap are indicated by dots.

920

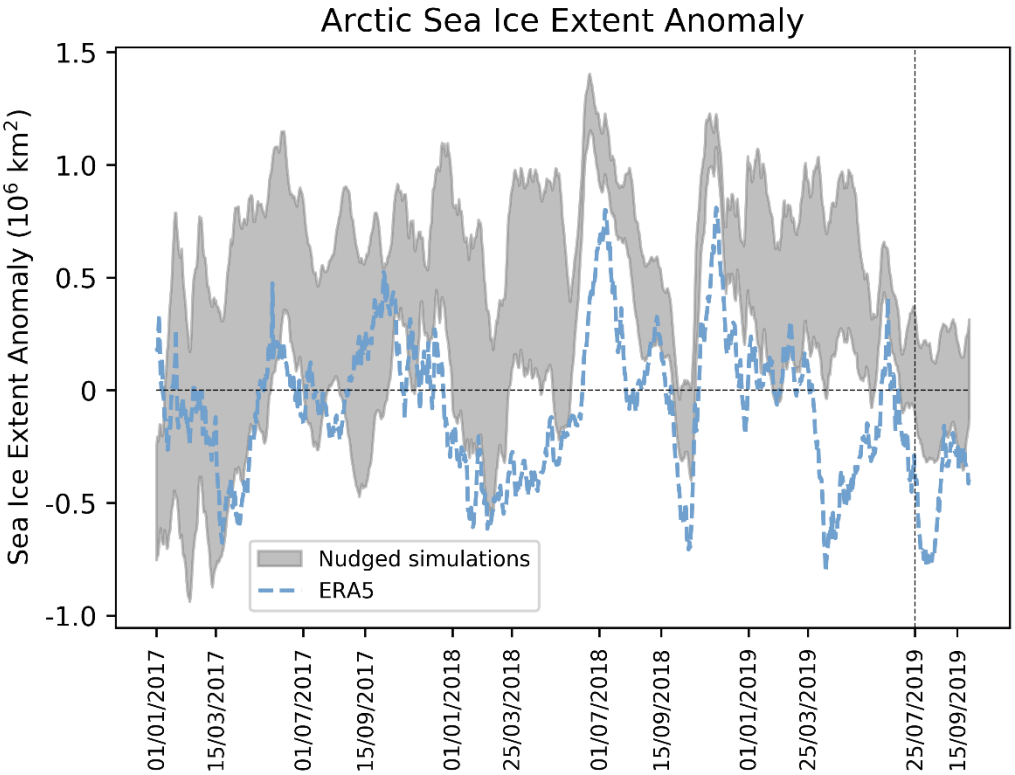

Figure 14. Arctic sea ice extent anomalies (climatology computed using the 2007–2016 period) from ERA5 (blue solid line) and the present-day nudged simulation. The peak of the European heatwave on 25 July 2019 is marked by the vertical dashed line.

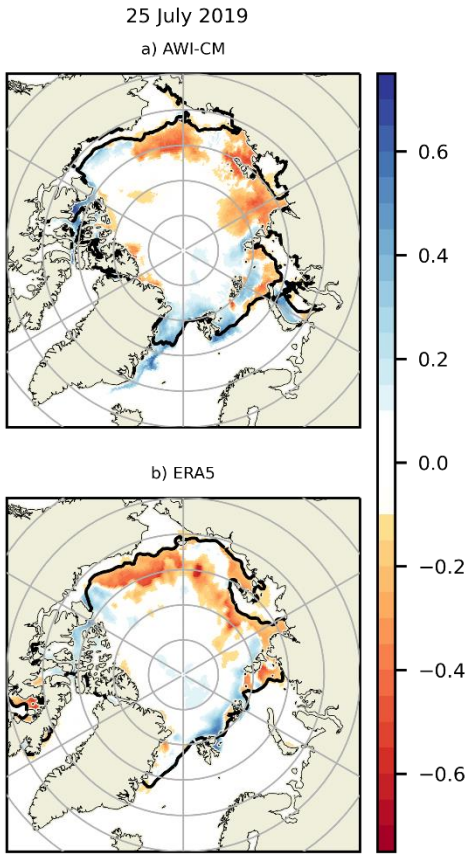

929

930 Figure 15. SIC anomalies (climatology computed using the 2007-2016 period) on 25th July
931 2019 from (a) AWI-CM nudged simulations and (b) ERA5. Black contours show the
932 respective climatological 15% sea-ice concentration.

933

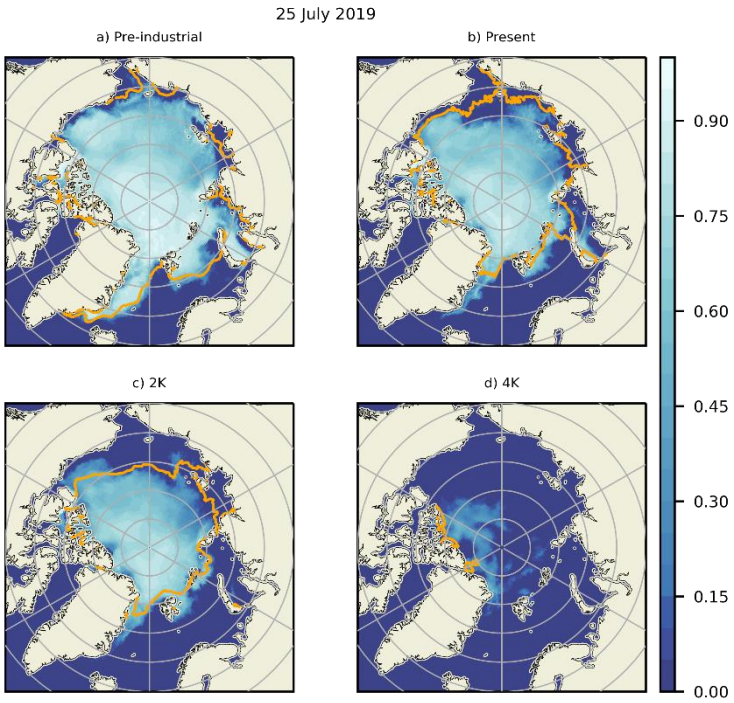

934

935 Figure 16. Sea ice concentration on 25th July 2019 from AWI-CM nudging experiments for
936 different climates: (a) pre-industrial, (b) present-day, (c) 2K warmer world and (d) 4K warmer
937 world. Orange contours show the respective climatological 15% sea-ice concentration contour.

938

939

940

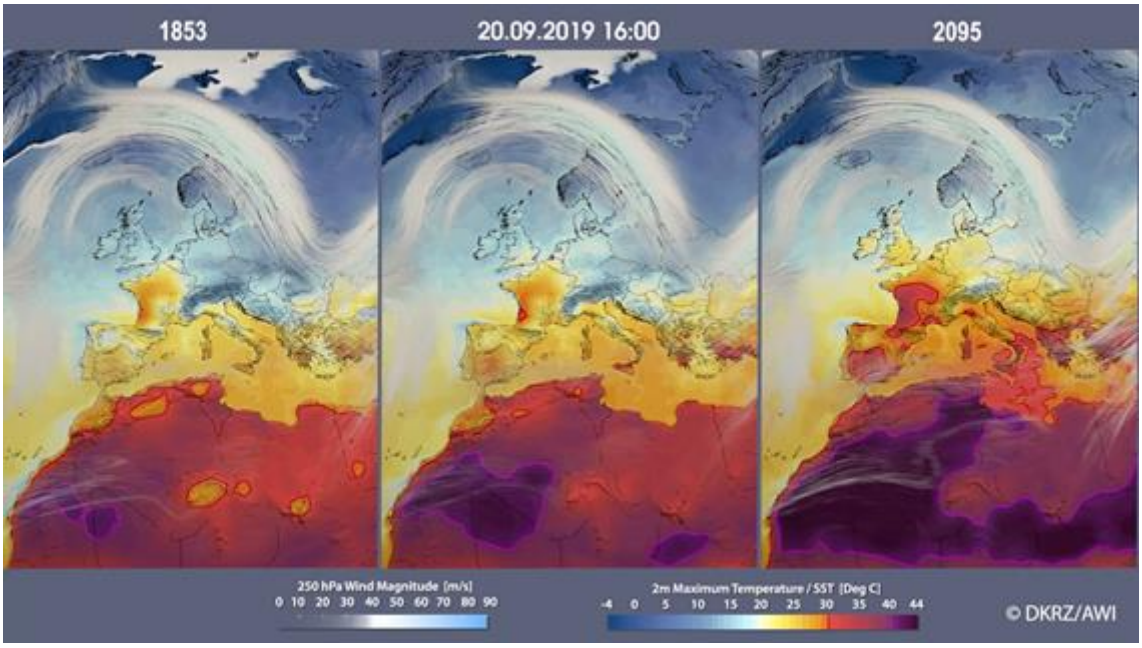

941

942 Figure 17. Storyline simulations of maximum 2m temperature, sea-surface temperature, sea ice
943 and 250 hPa winds at 1600 UTC on 20 September 2019: (left) for a pre-industrial climate,
944 (middle) present-day conditions, and (right) a 4K warmer world. 30C and 40C isotherms are
945 indicated by red and purple bold contours, respectively.

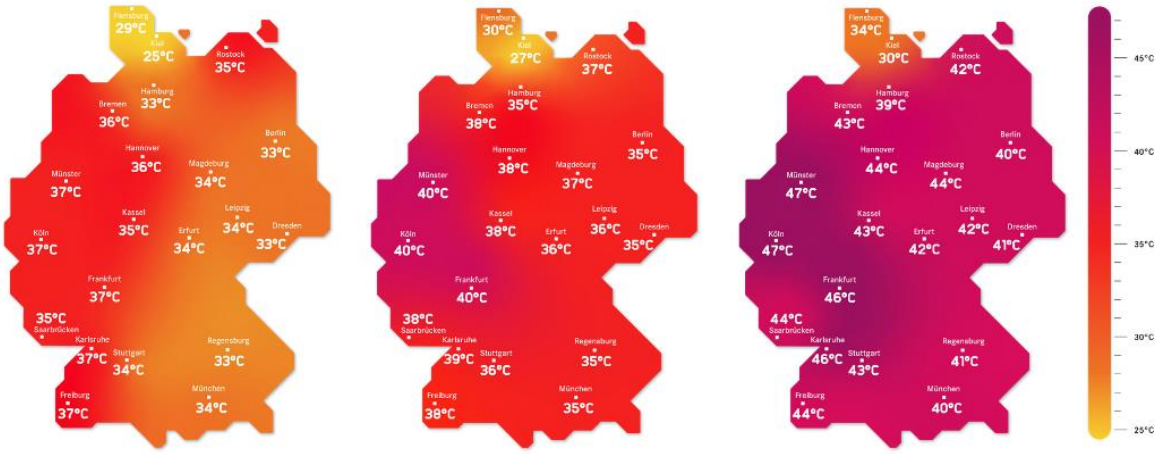

946

947 Figure 18. Schematic maps of 2m temperature for weather conditions in Germany at 1500 UTC
948 on 25 July 2019: (left) for a pre-industrial climate, (middle) present-day conditions, and (right)
949 a 4K warmer world. The maps have been produced by graphic designers of the communication

team of the Helmholtz Climate Initiative using observed values for the locations shown on the map and by adding temperature increments from the storyline scenarios for pre-industrial and 4K warmer conditions.